Molecular Neurobiology (2019) 56:873–891
https://doi.org/10.1007/s12035-018-1103-z

Impaired Wnt Signaling in the Prefrontal Cortex of Alzheimer's Disease

Jonas Folke[1] · Bente Pakkenberg[1,2] · Tomasz Brudek[1]

Received: 25 January 2018 / Accepted: 1 May 2018 / Published online: 26 May 2018

Abstract

Wnt pathway is involved in synaptic plasticity and neuronal survival, and alterations in Wnt signaling have previously been reported both in aging and neurodegenerative diseases, including Alzheimer's disease (AD). This study sought to evaluate Wnt signaling pathway interplay integrity across prefrontal lobe structures in AD patients compared to normal aging. Using the open-access BrainCloud™ database, 84 gene expression profiles and clustering effect were analyzed in the dorsomedial prefrontal cortex (PFC) across a time span of 21–78 years of age. Next, expression levels of the selected genes were investigated in post-mortem brain tissue from 30 AD patients and 30 age-matched controls in three interdependent brain areas of the PFC. Results were assessed in relation to Braak stage and cognitive impairment of the patients. We found a general age-related factor in Wnt pathway genes with a group of genes being closely interrelated in their expression across the time span investigated in healthy individuals. This interrelation was altered in the AD brains studied, as several genes presented aberrant transcription, even though not always being altered at protein levels. Noteworthy, beta(β)-catenin and glycogen synthase kinase 3-beta (GSK3β) showed a dynamic switch in protein levels and activity, especially in the orbitofrontal cortex and the medial frontal gyrus. A significant decrease in β-catenin protein levels were inversely associated with increased GSK3β tyrosine activating phosphorylation, in addition to downstream effects associated with disease progression and cognitive decline. This study is the first that comprehensively evaluates Wnt signaling pathway in the prefrontal cortical lobe structures of AD brains, in relation to age-related coordinated Wnt signaling changes. Our findings further support that increased kinase activity of GSK3β is associated with AD pathology in the PFC.

Keywords Alzheimer's disease · Wnt signaling pathway · Glycogen synthase kinase 3-beta · Beta-catenin · Braak staging · BrainCloud™

Introduction

Alzheimer's disease (AD) is a neurodegenerative disorder and the leading cause of age-related dementia [1]. AD is accompanied by three main pathological changes: diffuse loss of neurons [2], intracellular deposits of tau protein called neurofibrillary tangles [3], and extracellular senile plaques mainly comprised of amyloid-beta peptides [4]. Five percent of all AD cases are linked to disease-associated mutations, whereas the etiology is unknown in remaining 95% of cases. Thus, AD is considered a multifactorial disease with age being the most important risk factor [5, 6]. AD is accompanied by progressive cognitive deterioration and prominent behavioral instabilities. In early stages, episodic memory deficits are followed by personality changes, most commonly apathy and/or disengagement, functions found to be related to the prefrontal cortex (PFC) [7–9].

Wnt signaling is comprised of highly conserved evolutionary branch of proteins across various species [10] and plays a pivotal role in cell self-renewal, proliferation, and maintenance of many types of tissues [11]. It is divided into two major branches: canonical (Wnt/β-catenin) and non-canonical [12]. The activation of either pathway depends on a complex interaction of 19 Wnt ligands, several agonists and antagonists, and receptors; hence, manifesting its modularity

Electronic supplementary material The online version of this article (https://doi.org/10.1007/s12035-018-1103-z) contains supplementary material, which is available to authorized users.

✉ Jonas Folke
Jonas.folke@regionh.dk

[1] Research Laboratory for Stereology and Neuroscience, Bispebjerg-Frederiksberg Hospital, University Hospital of Copenhagen, Nielsine Nielsens Vej 6B, Building 11B, 2nd floor, DK-2400 Copenhagen, Denmark

[2] Institute of Clinical Medicine, Faculty of Health, University of Copenhagen, Blegdamsvej 3B, DK-2200 Copenhagen, Denmark

properties to maintain cellular homeostasis. As reviewed by Inestrosa et al. [13], Wnt signaling has continuously been shown to play an important role in the central nervous system (CNS) throughout life. During embryonic CNS development, Wnt signaling has been reported to regulate neuronal self-renewal, polarity, axon branching, and synaptogenesis [14, 15]. Many Wnt components are expressed in various parts of the brain, e.g., the PFC and cerebral cortex, hippocampus, and the olfactory bulb [16], and have been shown to be involved in several neurological disorders, e.g., mental and mood disorders as well as several cancers [10, 17]. These facts underlie the post-natal importance of the pathway in normal brain function.

Alterations in expression of the Wnt components have recently drawn attention in relation to aging both in health and disease. With respect to normal aging, the dysregulations are very dependent on cell types such as an increased transcription through the canonical pathway in artery cells [18], whereas a downregulation is observed in skeletal cells [19]. Wnt signaling has also been shown to decline with age in the rat brain [20]. Dysregulation of Wnt has also been associated with age-related diseases, e.g., osteoporosis [21], colon cancer [22], Parkinson's disease [23], and AD [24]. The latter is supported by vast studies in the past decade, suggesting that changes in Wnt pathway are a characteristic pathological hallmark of AD [13, 17, 25].

Several Wnt signaling components have been found to be altered in both familial and sporadic cases of AD. In familial cases of AD, carrying the presenillin-1 (PS-1) mutation results in a reduction of β-catenin and, additionally, the familial PS-1 mutant expression leads to increased GSK3β activity [26]. Extended research has been carried out in sporadic AD cases without apparent genetic involvement. The overall deduction suggests an repressed Wnt signaling in the AD brains; partly explained by increased GSK3β activity which increases tau protein phosphorylation [27], decreased β-catenin gene and/or protein expression [28, 29], increased Dickkopf-1 (DKK1) in AD [24], and increased DKK-3 in cerebrospinal fluid and plasma from AD patients [30]. The co-receptor low-density-related protein 6 (LRP6) has also been shown to be reduced in AD cases [28, 29]. Interestingly, a splice variant of LRP6 was associated with AD [31], and a single nucleotide polymorphism in the LRP6 was correlated with decreased β-catenin signaling in late onset AD cases [32], linking sporadic cases with Wnt signaling genetics.

Wnt signaling and especially GSK3β are of great interest due to its previous therapeutic potential in bipolar affective disorder as a molecular target of lithium [33].

To further understand the discrepancy in AD pathology, we first examined the aging effect on Wnt signaling gene expression in cognitively normal aging individuals in the PFC using the public available database, BrainCloud™. Following, we investigated expression of Wnt components in three connected areas in the PFC in AD patients compared to age-matched control group. We assessed transcription levels of 84 genes that are related to Wnt signaling pathway and the possible translation into protein expression and post-translational modifications. The findings from this study are important for understanding the Wnt signaling pathology in AD and to elucidate the potential aging effects on Wnt signaling.

Results

Wnt Signaling Pathway Gene Expression Shows a Divergent Picture During Healthy Aging

Table S1 lists the 84 genes that were included in this study which represent the assessed pathway in the pathology in AD, including gene names, gene abbreviations, and chromosomal location. The following gene expression levels were found to be negatively correlated with age: *APC*, *CSNK1A1*, *FZD2*, *FZD3*, *MAPK8*, *NLK*, *WNT2B_1*, *WNT6*, and *WNT7A* (Fig. 1a), whereas *AES*, *CCND1*, *EP300*, *FBXW4*, *FRAT1*, *GSK3B*, *LRP6*, *SFRP1*, *TLE1*, and *VANGL2* were found to be increased during aging (Fig. 1b). Table 1 summarizes gene expression levels correlated with age.

Cooperative Clustered Gene Expression Correlates During Healthy Aging

Spearman's correlation matrices associating all genes were visualized within the aging interval (Fig. 2). Heat map with incorporated hierarchical cascade clustering identifies Wnt pathway genes, which are potentially coordinated within their transcription, indicating relatedness. Four different clusters of highly intercorrelated genes were identified during aging: cluster 1: *DKK1*, *CTNNB1*, *CSNK1A1*, *DIXDC1*, *WNT2B_2*, *MAPK8*, *CSNK2A1*, *WNT16*, *BTRC*, *PRICKLE1*, *FZD3*, *APC*; cluster 2: *RUVBL1*, *WNT7B*, *SOX17*, *AXIN1*, *WIF1*, *FZD8*, *FZD2*, *FZD1*; cluster 3: *WNT11*, *WNT3A*, *PITX2*, *DVL1*, *FOXN1*; cluster 4: *AES*, *FBXW4*, *FZD9*, *NFATC1*, *EP300*, *FOSL1*, *TCF7L1*. Interestingly, none of the genes in the clusters show close chromosomal proximity, thus, indicating non-genomic clustering effect during aging. The clustering shows synchronized gene transcription during aging. The most significant pairwise correlations ($|r| > 0.60$) are given in Table 2.

Significant Correlations Between Pairs of Genes Located on the Same Chromosomal Band During Aging

Nine groups of genes were found in near proximity, as evaluated by the band location: *CTNNB1* and *DVL1* (1p36); *WNT6* and *WNT10A* (2q35); *LEF1* and *PITX2* (4q25); *TCF7* and

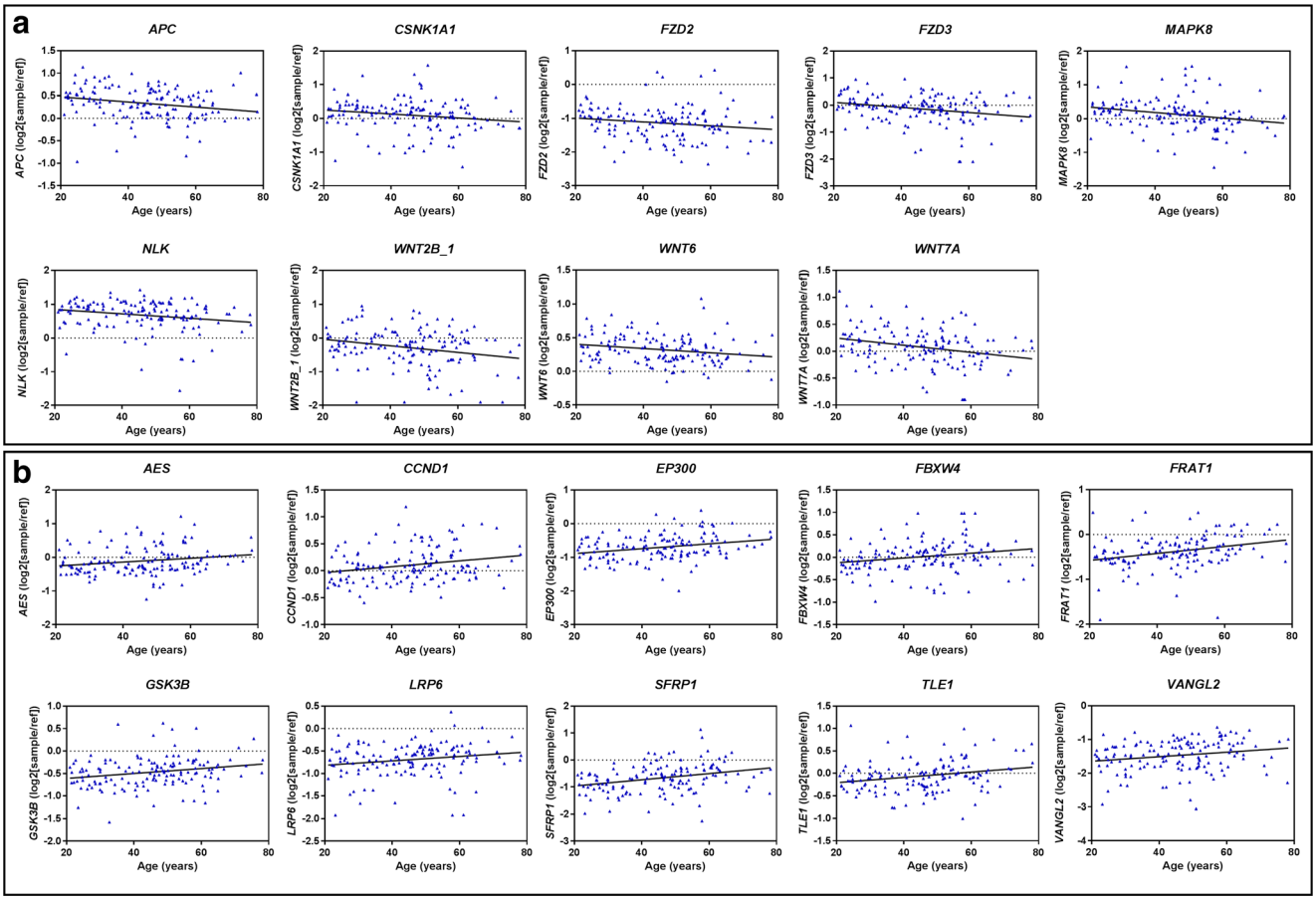

Fig. 1 Significant linear regressions of Wnt pathway related gene expression levels during healthy aging from BrainCloud™ data. Scatterplots present relative gene expression levels. **a** Significant, negatively correlated and **b** significant, positively correlated as a function of age in years. Blue triangles represent healthy individuals in the aging interval. The black line represents linear regressions and the dotted line represents the log2[sample / reference genes] = 0

WNT8A (5q31); *BTRC*, *FBXW4* and *FRAT1* (10q24); *CCND2*, *LRP6* and *WNT5B* (12p13); *EP300* and *WNT2B* (22q13); *CCND1*, *FGF4*, *FOSL1*, *LRP5* and *WNT11*; and *MYC* and *WISP1* (8q24). Further evaluations showed that three gene pairs share the same chromosomal sub-band: *CCND2* and *WNT5B* (12p13.3); *CCND1* and *FGF4* (11q13.3); and *MYC* and *WISP1* (8q24.2). A single gene pair shared same chromosomal sub-sub-band: *BTRC* and *FBXW4*

Table 1 Wnt pathway gene expression correlation with age

Decreased with aging			Increased with aging		
Gene	Correlation	Adjusted *p* value	Gene	Correlation	Adjusted *p* value
FZD2	− 0.213	1.55E−05	*EP300* #	0.270	9.98E−06
WNT2B	− 0.189	8.00E−04	*CCND1*	0.229	8.00E−04
FZD3	− 0.227	9.00E−03	*VANGL2*	0.225	8.00E−04
NLK	− 0.217	7.00E−03	*GSK3B*	0.233	2.00E−04
CSNK1A1	− 0.252	6.00E−03	*FRAT1* #	0.359	9.00E−03
WNT7A[a]	− 0.276	6.00E−03	*SFRP1* #	0.305	7.00E−03
MAPK8	− 0.243	2.30E−02	*FBXW4*	0.278	5.00E−03
WNT6	− 0.224	1.00E−02	*AES*	0.235	1.00E−03
			LRP6	0.217	1.00E−03
			TLE1	0.264	1.00E−03

[a] Pearson correlation. Otherwise Spearman's. Only significant adjusted *p* values are shown in the table. Data is for multiple comparisons using Benjamini-Hochberg

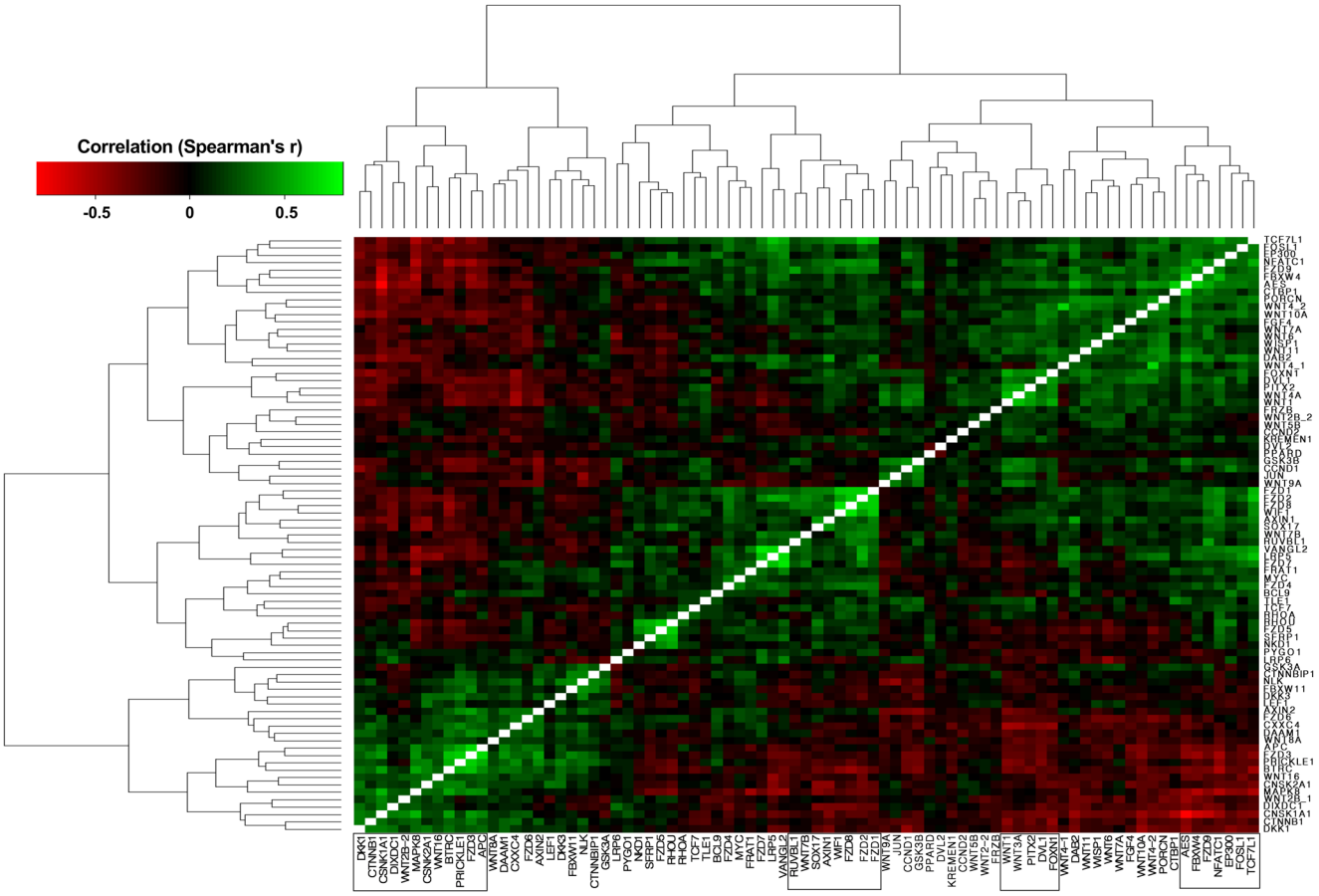

Fig. 2 Heat maps for pairwise correlations of genes during aging. Heat map showing Spearman's correlation matrices of pairwise gene expression correlations using hierarchical clustering within aging interval with length representing gene relatedness. Boxes represent significant clustering's ($p < 0.05$)

(10q24.32). Following Bonferroni corrected analyses at $p = 0.002$, only expression levels for *FOSL1* and *LRP5* were positively correlated with aging (Spearman $r = 0.415$, $p < 0.001$). No other gene pairs or gene groups were significantly correlated with aging (Table S2).

Transcriptional Profiling of Wnt Signaling Related Genes in AD Pathology

To gain insight into gene expression changes in AD past aging effects, we performed a transcriptional profiling of 84 Wnt signaling related genes using the human RT^2 profiler PCR array. Results from the profiling are presented as a heat map (Fig. 3) and describe the difference between AD patients and corresponding normal controls in brain samples from the OFC, MFG, and SFG. Gene expression levels of six genes were under the limit of detection in either group and thus excluded from the microarray analyses, i.e., *FGF4*, *FOXN1*, *MMP7*, *PITX2*, *WNT3A*, and *WNT16* (Table S1, highlighted in red). In total, 21 genes (25%) were differentially expressed, e.g., having a fold change $\geq \leq 2.0$ in the AD patients compared to control subjects (Table 3). Hierarchal cluster analysis shows two significant alignments in the three brain areas ($p < 0.05$) (Fig. 3). Evaluating the clusters, the OFC showed an increased expression in the cluster containing the genes *WNT10A*, *WNT11*, and *WNT7B*, compared to the MFG and SFG. The second cluster containing the genes *FZD3*, *CSNK2A1*, *PRICKLE1*, *DKK1*, *WIF1*, and *RHOA* shows similarities of unaffected gene expression levels in the OFC and MFG, in contrast to the SFG which showed decrease in expression levels compared to controls. These results suggest a regional expression pattern conformation in the signaling pathway in AD pathology. The hierarchical clustering between regions shows a closer connectedness between the OFC and MFG.

Validation of Microarray Profiling on Single Sample Gene Targeting Using qPCR

To validate the microarray findings, all significant profiling hits from the RT^2 profiler PCR array were selected for

Table 2 Highly significant ($|r| > 0.60$) pairwise correlation during aging interval

Gene 1	Gene 2	Correlation	p value
AES	*CSNK1A1*	− 0.807	2.62E−34
FZD7	*VANGL2*	0.727	5.87E−25
FZD8	*WIF1*	0.721	1.99E−24
APC	*FZD3*	0.698	2.40E−22
LRP5	*VANGL2*	0.692	7.09E−22
WNT4_1	*WNT4_2*	0.673	2.38E−20
FZD1	*FZD8*	0.652	9.16E−19
AES	*FBXW4*	0.652	7.49E−19
FZD3	*PRICKLE1*	0.637	9.89E−18
FZD1	*FZD2*	0.639	6.54E−18
AES	*CTBP1*	0.642	4.16E−18
FZD5	*RHOU*	0.644	3.21E−18
CSNK1A1	*FBXW4*	− 0.651	1.09E−18
FZD2	*FZD8*	0.625	6.03E−17
FZD7	*LRP5*	0.606	7.89E−16
BTRC	*FZD3*	0.609	5.00E−16
FZD1	*WIF1*	0.619	1.29E−16
LRP5	*TCF7L1*	0.602	1.50E−15
FZD2	*TCF7L1*	0.602	1.45E−15

qPCR validation. Additionally, we included Wnt pathway genes that were previously shown to be deregulated in AD pathology, namely, *CTNNB1*, *GSK3B*, *LRP6*, and *LRP6Δ3* [28, 31]. *WNT7B* was also included due to close proximity to twofold increase and previously reported indication of an involvement in AD [29]. Reverse transcription quantitative real-time PCR (RT-qPCR) was performed on all genes sub-divided into their cellular compartmentalization. The succeeding validation of gene expression confirmed significant alterations of three genes (Fig. 4a), the *WIF1* antagonist in the OFC (fold change (FC) = − 0.31; $p = 0.002$) and MFG (FC = − 0.39; $p = 0.034$), the ligands *WNT2B* in the SFG (FC = + 2.04; $p = 0.033$), and *WNT7B* in the OFC (FC = − 0.33; $p = 0.042$). Receptor alterations were observed (Fig. 4b) in the *FZD2* gene in the MFG (FC = + 3.37; $p = 0.003$), similarly the *FZD3* was shown to be increased in the OFC (FC = + 2.72; $p = 0.004$). In addition to the receptors, the co-receptor *LRP5* was significantly increased in the OFC (FC = + 6.29; $p = 0.006$) and SFG (FC = + 2.71; $p = 0.005$) and somewhat increased in the MFG (FC = + 1.75; $p = 0.072$). Downstream of the receptors, the intracellular gene *APC* was found to be increased in the SFG (FC = + 1.89; $p = 0.018$) (Fig. 4c), whereas the gene *RHOA* was downregulated in the OFC (FC = − 0.31; $p = 0.008$), the MFG (FC = − 0.60; $p = 0.049$), and close to significant decrease in the SFG (FC = − 0.68; $p = 0.062$). The subsequent nuclear gene expression changes were narrowed to the FOSL1 gene in the SFG (FC = + 2.43; $p = 0.016$) (Fig. 4d). The expression levels of all other genes were unchanged (Fig. S1). Based on previous results showing a significant correlation between *FOSL1* and *LRP5* due to chromosomal proximity, correlation analyses were made in all analyzed brain areas in healthy controls and AD. No significant correlations were found (data not shown).

Regional Expression Profiling Is Restricted to Disease Pathology

In AD, a sub-set of genes was found to be significantly disparate expressed between the three regions (Fig. 5a). The following genes: *CSNK2A2* (increased: OFC > MFG, decreased: SFG < OFC and MFG, $p < 0.001$), *PPARD* (decreased: SFG, $p < 0.0001$), *RHOA* (decreased: SFG, $p = 0.001$), *WNT2B* (decreased: SFG, $p < 0.001$), and *WNT5A* (increased: MFG > OFC and SFG < OFC and MFG, $p = 0.002$) levels were significantly decreased in the SFG compared to either OFC and MFG or both (Fig. 5a) in samples from AD brains. The non-demented controls showed no difference in gene expression levels between the three regions after applying Bonferroni correction (corrected p value being 0.002) (Fig. 5b). These novel results suggest a disease-specific discrepancy of Wnt signaling pathway-related gene expression levels in AD pathology.

Alterations in Protein Expression Levels in AD Patients

To assess if the observed aberrations in Wnt signaling gene expression levels are translated into changes in protein levels, we have performed single protein evaluations using western blotting. We observed that five proteins were deregulated in AD pathology compared to control subjects including proteins not involved in the main regulatory effects of the Wnt signaling pathway (Fig. 6). The protein levels of the following two ligands were found to be decreased; WNT2B (43%, $p = 0.022$) (Fig. 6g) and WNT7B in the OFC (29 kDa: 44%, $p = 0.021$; 39 kDa: 41%, $p < 0.001$) (Fig. 6i, j). For WNT7B, two bands were at 29 and 37 kDa (Fig. 6k) and were analyzed separately based on previous studies [29]. Furthermore, FZD3 receptor levels were decreased in the MFG (43%, $p = 0.003$) and SFG (46%, $p = 0.009$)

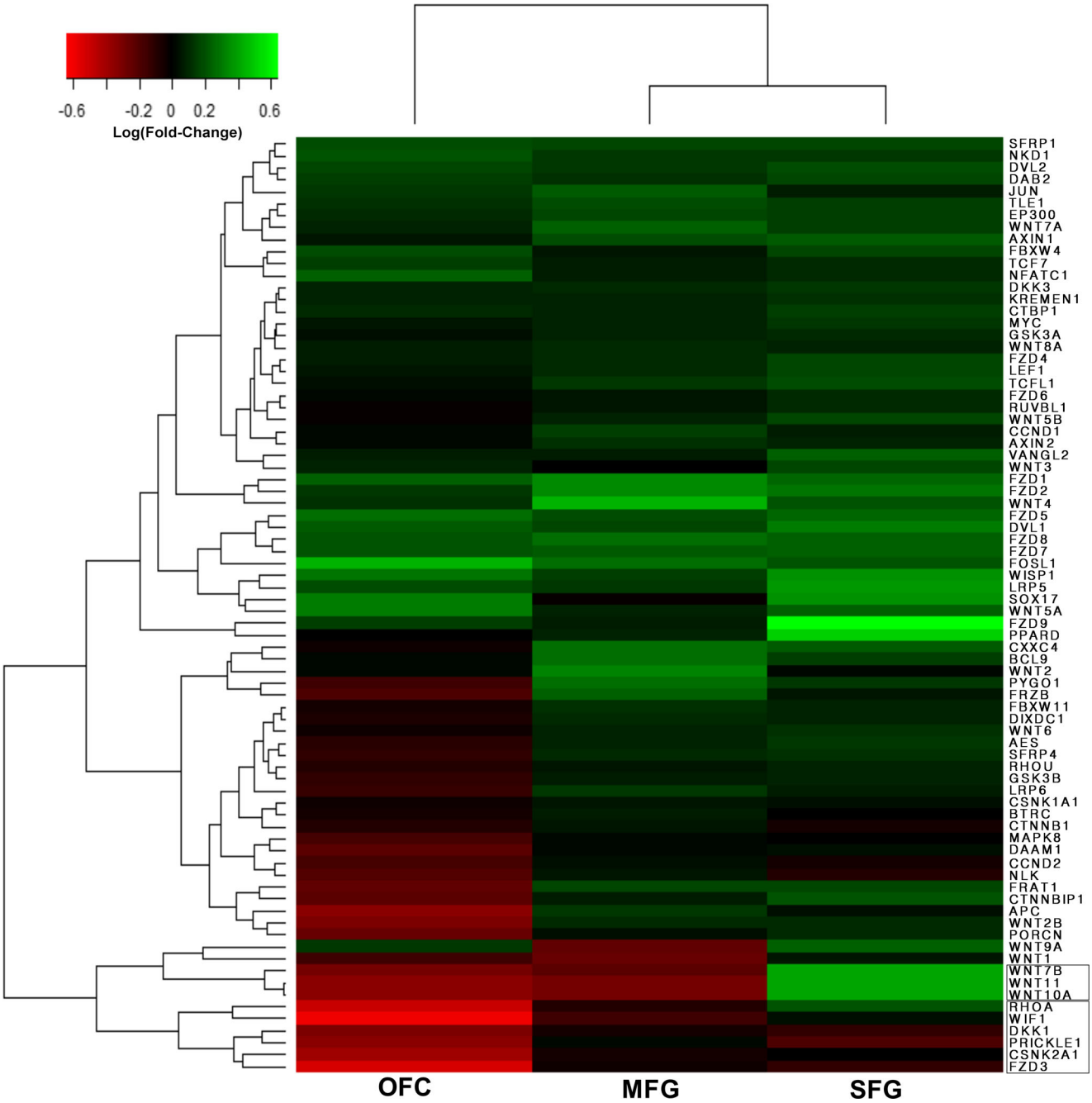

Fig. 3 Heat map representing RT^2 profiler PCR Microarray of Wnt Signaling pathway related genes. Hierarchical clustering of $\log_2$ (fold change) gene expression levels in AD patients compared to controls in all three brain regions, the superior frontal gyrus (SFG), the medial frontal gyrus (MFG), and the orbitofrontal cortex (OFC). Each row represents an investigated brain region. Significant clusters are represented by a box surrounding genes in left column ($p < 0.05$). Red represents decreased and green represents increased gene expression levels

(Fig. 6d). The intracellular protein RHOA expression was decreased correspondingly to the gene expression levels in the OFC (54%, $p = 0.009$), however, not in the MFG (50%, $p = 0.088$) (Fig. 6f). The nuclear protein FOSL1 (alternatively called FRA-1) levels were decreased in the MFG (56%, $p = 0.042$). Levels of APC, FZD2, LRP5, and WIF1 proteins were unchanged on translational level in AD brains (Fig. 6).

Aberrant Intracellular Wnt Signaling Activity in the Orbitofrontal Cortex and the Adjacent Region, the Medial Frontal Gyrus, in AD Cases Is Linked to Increased GSK3β Activity

The total levels of GSK3β were unchanged in all three areas of AD brains. The activity of GSK3β is known to be regulated by its phosphorylation at tyrosine 216 (pTyr216) [34]. The

Table 3 Profiling hits of Wnt signaling pathway array and RT-qPCR validation

Gene	GenBank	Functional gene name	Fold change (microarray)	Fold change (RT-qPCR)
Orbitofrontal cortex				
DVL1	NM_004421	Disheveled, dsh homolog 1 (*Drosophila*)	2.01	NS
FZD9	NM_003508	Frizzled family receptor 9	6.38	NS
LRP5	NM_002335	Low density lipoprotein receptor-related protein 5	2.41	6.29
PPARD	NM_006238	Peroxisome proliferator-activated receptor delta	3.24	NS
WNT7b	NM_058238	Wingless-type MMTV integration site family, member 7B	1.96	0.33
Medial frontal gyrus				
FOSL1	NM_005438	FOS-like antigen 1	1.91	NS
FZD1	NM_003505	Frizzled family receptor 1	2.20	NS
FZD2	NM_001466	Frizzled family receptor 2	7.70	3.37
WNT2	NM_003391	Wingless-type MMTV integration site family member 2	2.15	NS
WNT4	NM_030761	Wingless-type MMTV integration site family member 4	2.76	NS
Superior frontal gyrus				
APC	NM_000038	Adenomatous polyposis coli	0.46	1.89
CSNK2A1	NM_001895	Casein kinase 2, alpha 1 polypeptide	0.40	NS
DKK1	NM_012242	Dickkopf homolog 1 (*Xenopus laevis*)	0.49	NS
FOSL1	NM_005438	FOS-like antigen 1	2.80	2.43
FZD3	NM_017412	Frizzled family receptor 3	0.30	NS
FZD9	NM_003508	Frizzled family receptor 9	2.11	NS
PRICKLE1	NM_153026	Prickle homolog 1 (Drosophila)	0.46	NS
RHOA	NM_001664	Ras homolog gene family, member A	0.32	0.68
WIF1	NM_007191	WNT inhibitory factor 1	0.25	NS
WNT2B	NM_004185	Wingless-type MMTV integration site family, member 2B	0.50	2.04
WNT5A	NM_003392	Wingless-type MMTV integration site family, member 5A	2.01	NS

NS: not significant

phosphorylated pTyr216-GSK3β levels were only increased in the MFG (190%; $p = 0.027$) (Fig. 7b). The ratio of phosphorylated pTyr216-GSK3β to the total GSK3β levels indicates a high increase of GSK3β activity in the OFC (308%; $p = 0.028$) and MFG (279%; $p = 0.029$) (Fig. 7c). GSK3β is inhibited through phosphorylation of serine 9 (pSer9) [34], and a significant decrease in the total amount of pSer9-GSK3β in the OFC (28%; $p = 0.007$) (Fig. 7d) was observed; however, no changes were observed in the ratio pSer9-GSK3β/total GSK3β (Fig. 7e). No differences in GSK3β expression or post-translational levels were observed in AD SFG (Fig. 7a); however, a significant increase was observed in the GSK3β isoform, GSK3α, restricted to the SFG region (295%; $p = 0.002$) in AD patients (Fig. 7f).

The Aberrancy of GSK3β Activity Is Preceded by Changes in the Total β-Catenin Levels Explained by Reduced Nuclear Locating Phosphorylation and Increased Degradation

The GSK3β downstream target β-catenin was found to be decreased in AD patients in the OFC (43%; $p = 0.037$) and MFG (58%; $p = 0.040$) (Fig. 8a), possibly as a result of the increased GSK3β activity, which regulates β-catenin phosphorylation at serine 45 (pSer45) [35]. Once phosphorylated at Ser45, β-catenin is directed for proteasomal degradation. The total amount of pSer45-β-catenin was unaffected in AD patients compared to controls in all regions (Fig. 8b). However, the ratio of pSer45-β-catenin/total β-catenin was significantly increased in the MFG (207%; $p = 0.003$) and close to significance in the OFC (230%; $p = 0.059$) in AD patients (Fig. 8c). When GSK3β is inactive, the β-catenin is translocated to the nucleus by a phosphorylation at Ser675 (pSer675) [35]. The total levels of nucleus targeted pSer675-β-catenin was significantly decreased in the MFG (36%; $p = 0.020$), whereas the pSer675-β-catenin in the OFC is not significantly decreased (42%, $p = 0.070$) in AD (Fig. 8d). The ratio of pSer675-β-catenin/total β-catenin was insignificantly decreased in the OFC (40%, $p = 0.136$) and MFG (36%, $p = 0.134$) (Fig. 8e) in AD. Hence, the observed increase in GSK3β activity seems to have a direct effect on the increased degradation and reduced nuclear translocation of β-catenin in the OFC and MFG.

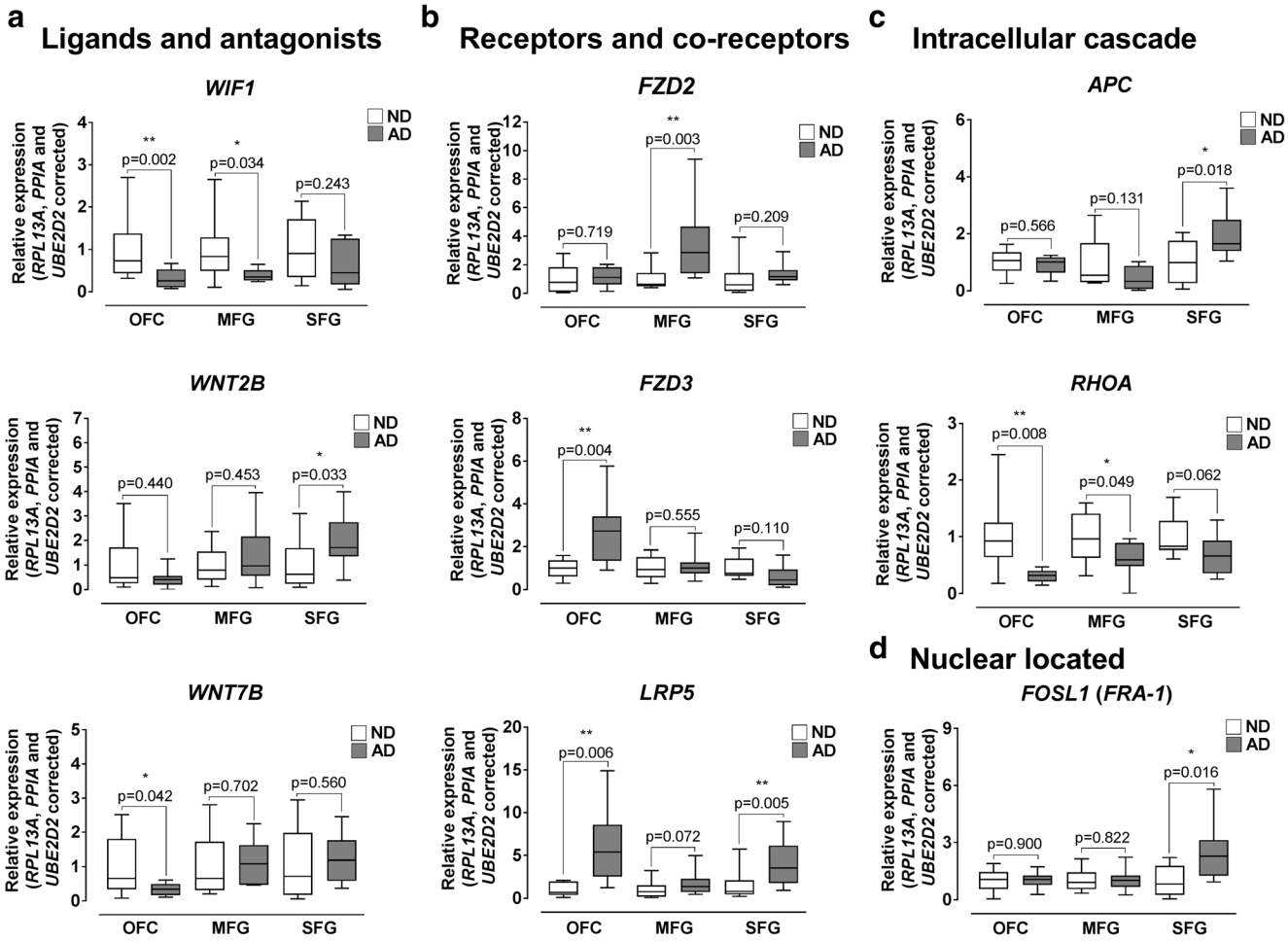

Fig. 4 Relative mRNA expression levels of significant findings from profiling hits on microarray. Box and whisker plots of significant Wnt signaling pathway gene expressions at the level of **a** ligand and antagonists, **b** receptors and co-receptors, **c** intracellular cascades, and **d** nuclear located the in orbitofrontal cortex (OFC), medial frontal gyrus (MFG), and superior frontal gyrus (SFG). Gene expression ratios with the minimum, the maximum, the median value, and the 25th, 50th, and 75th percentiles are shown for non-demented controls (ND: white) and Alzheimer's disease (AD: gray) brains. The relative expression is normalized to *RPL13A*, *PPIA*, and *UBE2D2*. $*p < 0.05$, $**p < 0.01$

Correlation Between RNA Levels and Protein Expression

Subsequent evaluation demonstrated that small number of Wnt signaling gene transcription levels can be correlated with corresponding protein expression levels, summarized in Table 4. The *WNT7B* gene expression was positively correlated in the OFC with the total WNT7B protein levels (39 kDa: $r = 0.484$; $p = 0.042$). Further, the *CTNNBP* gene expression levels were negatively correlated to the phosphorylated β-catenin at Ser45 ($r = -0.408$; $p = 0.041$) in the OFC. No further correlations were observed.

Changes in Gene and Protein Levels Are Correlated to Disease Progression and Cognitive Impairment

The pathology annotation of AD is defined by post-mortem Braak staging from I (1) to VI (6), whereas the cognitive capabilities is screened by the Mini-Mental State Examination (MMSE), only available for the OFC samples. After Bonferroni correction for multiple comparisons, the *FZD3* ($r = 0.622$; $p = 0.004$) and *WIF1* ($r = -0.670$; $p = 0.002$) gene expression levels and WNT7B protein levels (39 kDa: $r = -0.795$; $p < 0.001$) in the OFC were significantly correlated to disease severity defined by Braak staging in AD (Fig. 9). Interestingly, the WNT7B protein was also correlated with the MMSE scale (39 kDa: $r = -0.795$; $p < 0.003$) (Fig. 9).

Discussion

Wnt signaling has previously been investigated in aging and also as a possible factor contributing to the pathogenesis in AD [25, 36–38]. The present study is the first to evaluate the effect of aging on the Wnt signaling pathway in the dorsolateral PFC of brains from healthy subjects using the

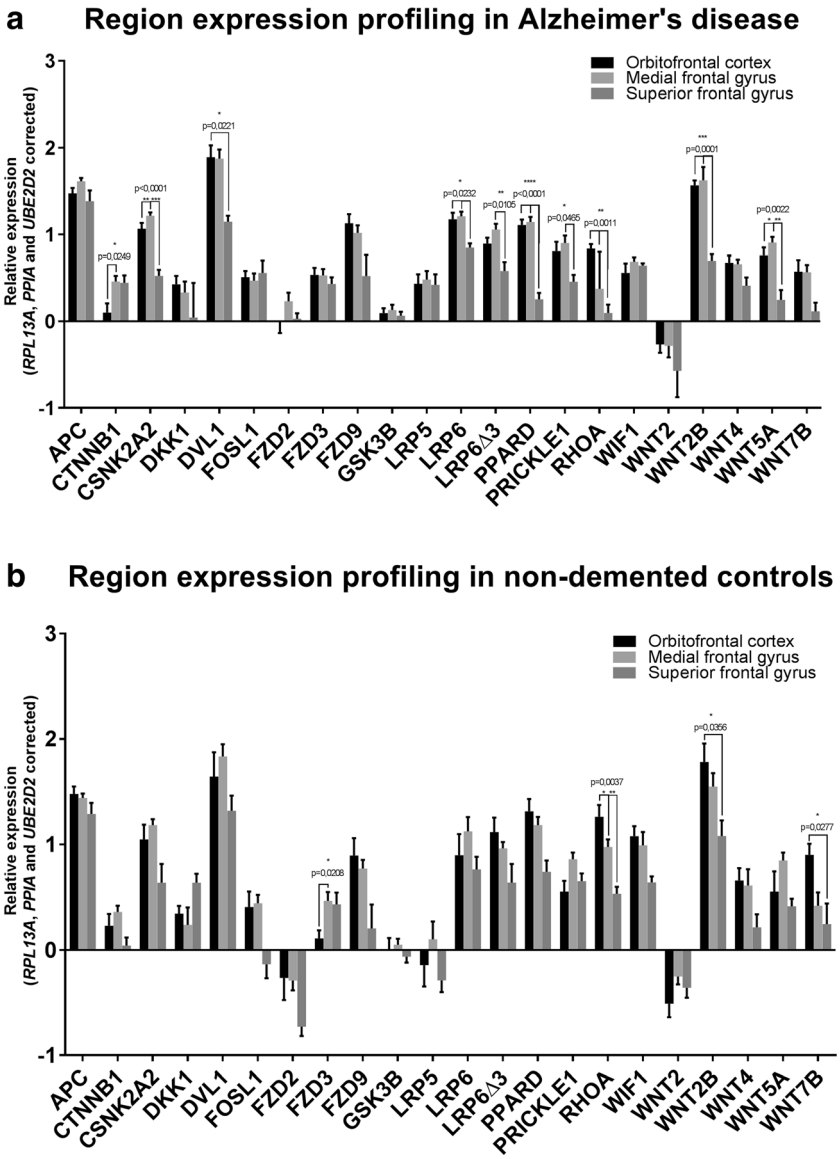

Fig. 5 Bar plot showing regional gene expression differences in Alzheimer's disease (**a**) and non-demented controls (**b**) in the orbitofrontal cortex (Black), the medial frontal gyrus (light gray), and superior frontal gyrus (dark gray). The relative expression levels are normalized to *RPL13A*, *PPIA*, and *UBE2D2*. Data depict mean ± SEM. One-way ANOVA p values: *$p < 0.05$, **$p < 0.01$, *** $p < 0.001$, **** $p < 0.0001$ are indicated

BrainCloud™ database [39] to unravel the interconnectedness Wnt signaling gene expression. Following analyses of the healthy brain, we established a comprehensive Wnt profile in three connected regions of the human PFC in AD patients, e.g., the orbitofrontal cortex (OFC), the medial frontal gyrus (MFG), and the superior frontal gyrus (SFG). The dorsolateral PFC and MFG have interconnected anatomy [40]. Among 84 genes, we identified a sub-set which was deregulated following aging. Of those, the *APC*, *FZD2*, *FZD3*, and *WNT2B* genes were downregulated as a part of human aging in the PFC. Interestingly, in AD patients, we found their expression levels to be increased despite the apparent discrepancy between brain regions suggesting a possible role in AD. The *FZD3* has previously been found to be downregulated in the posterior cingulate cortex of AD patients, while *WNT2B* was reported deregulated in the hippocampus, the entorhinal cortex, and the MFG in AD patients [41].

Further, our results revealed significant, AD-related alterations in gene expression levels of the ligands *WIF1* and *WNT7B*, the co-receptor *LRP5*, the intracellular cascade gene *RHOA*, and the nuclear transcription factor-forming unit *FOSL1*. The exact role of *WIF1* in AD still remains unclear; nevertheless, *WIF1* gene expression has been shown to be increased in normal aging [42] and decreased in the temporal lobe in AD brains [43]. WNT7B has recently been found to be decreased in the entorhinal cortex and hippocampus [29] as well as important in synaptic regulation and remodeling [44]. Interestingly, *WNT7B* gene expression and protein levels were decreased in the OFC, and protein levels were further negatively correlated to increased Braak staging and to cognitive impairment in AD patient defined by the MMSE stage. These results could indicate a pivotal role of the WNT7B in the AD pathogenesis. Besides the WNT7B, the *FZD3* gene expression levels were positively correlated to Braak staging in the

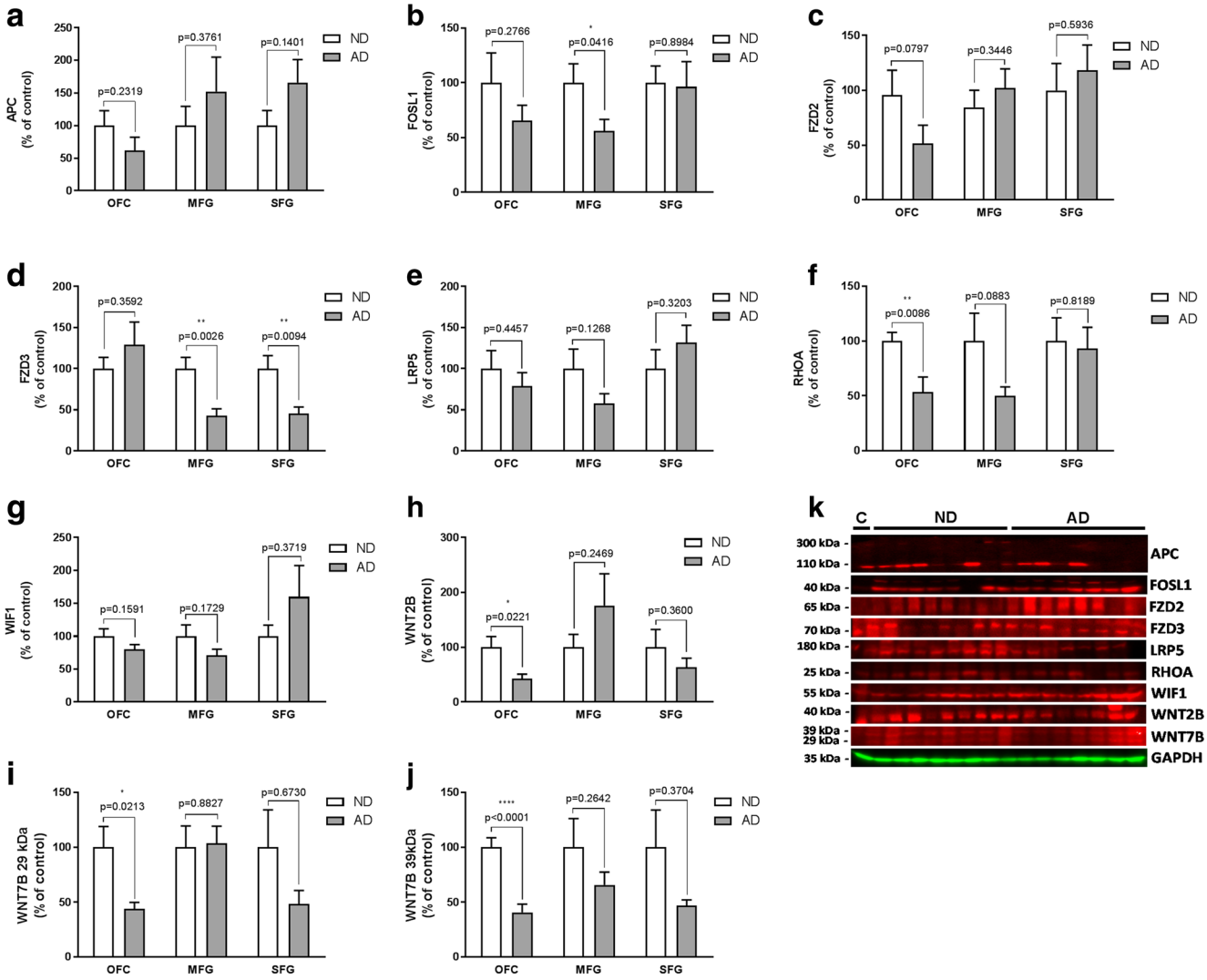

Fig. 6 Immunoblotting of Wnt proteins based on pathway-focused significant differences in Wnt expression. Western blot of the Wnt components **a** APC, **b** FOSL1, **c** FZD2, **d** FZD3, **e** LRP5, **f** RHOA, **g** WIF1, **h** WNT2B, **i** WNT7B 29 kDa, and **j** WNT7B 39 kDa. **k** Depict a minor representation of immunoblots of non-demented controls (ND) and Alzheimer's disease (AD) patients. Quantification of protein band intensities is normalized to GAPDH. Bar graphs shows % protein of ND (white) compared to AD (gray). Data depict mean ± SEM. $*p < 0.05$, $**p < 0.01$, $****p < 0.0001$ are indicated. C—pooled (calibrator) sample

OFC, whereas the *WIF1* gene expression levels were negatively correlated with the Braak staging in the OFC.

Moreover, we found a decreased gene expression of *RHOA* in the OFC and MFG in AD patients with a corresponding decrease in protein levels in the OFC. *RHOA* has previously been a target of interest in AD, due to its suggested role in synaptic function and plasticity [45], and has indeed been found to be decreased in the hippocampus of AD patients and in a transgenic mouse model [46].

Several genes cross-talk in different pathways; hence, we evaluated the pairwise correlation during aging to identify highly significant gene expression coherence. These pairwise correlations correspond largely to the cluster analysis with pairwise correlation placed in significant clusters, predominantly cluster two, including the pairwise correlated genes *APC*, *BTRC*, *FZD1*, *FZD2*, *FZD8*, and *WIF1*. In our microarray analyses of AD brains, only a few genes were grouped as in normal aging, e.g., *FZD3*, *CSNK2A1*, *PRICKLE1*, and *DKK1*, suggesting that the interaction in Wnt pathway gene regulation is disturbed in AD. One possible reason could be loci deregulation in AD. To rule out the effect of chromosomal co-localization, we compared expression levels of genes pairwise with same chromosomal localization. Interestingly, we found that only the *FOSL1* and *LRP5* (Table S2) were correlated; however, they did not share the same clustering group. The *FOSL1* and *LRP5* showed a comparable increase in the SFG from ND and AD patients, suggesting a pairwise regulatory mechanism, not apparent in the OFC and MFG. *LRP5* has been showed to have a neuroprotective effect by decreasing a pathological increased tau protein aggregation in

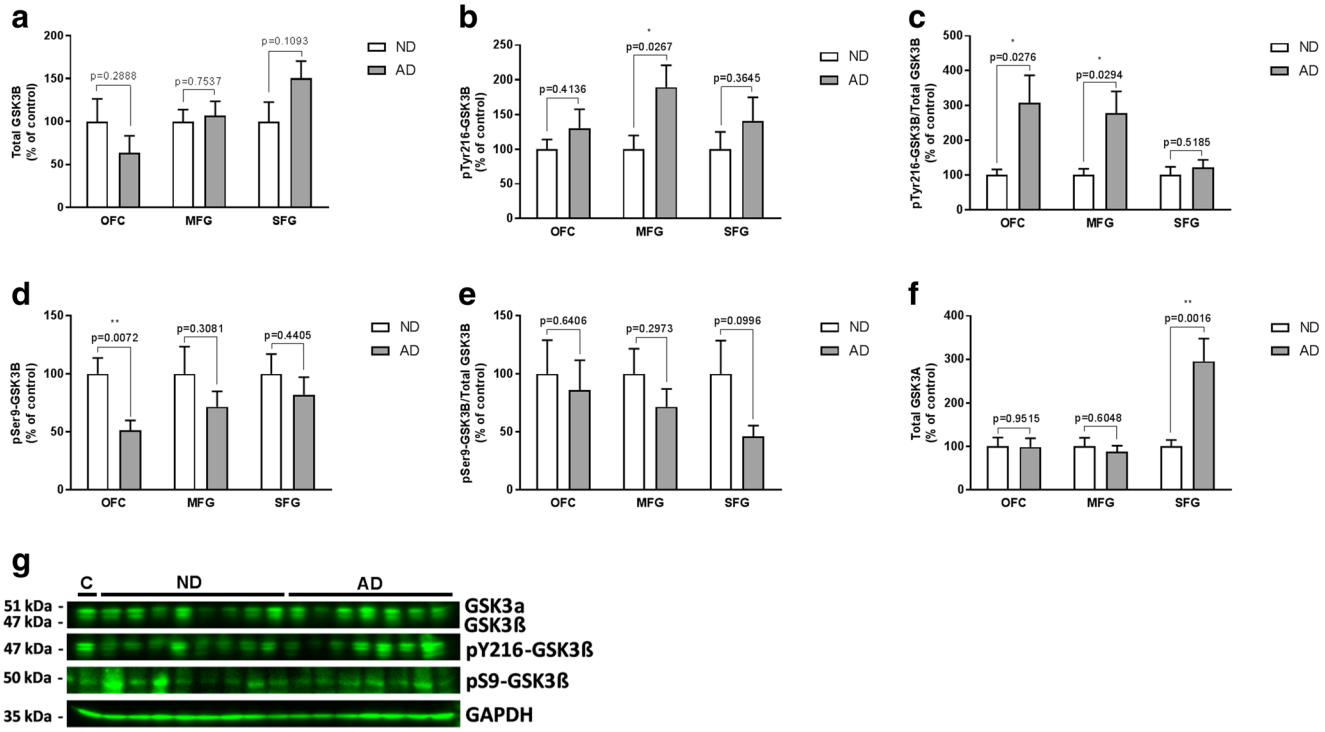

Fig. 7 Total level and phosphorylation of GSK3β and GSK3α. Western blot and quantification of **a** total GSKβ and its post-translational modifications on its **b** activating site phosphor-Tyrosine216 (pTyr216-GSKβ) and its **d** inhibitory site phosphor-ser9 (pSer9-GSKβ). **c** and **d** shows the post-translational modification intensities normalized to total GSKβ protein. **f** Shows GSK3α A protein. **g** Depict a minor representation of immunoblots of non-demented controls (ND) and Alzheimer's disease (AD) patients. Quantification of protein band intensities is normalized to GAPDH. Bar graphs shows % protein of ND (white) compared to AD (gray). Data depict mean ± SEM. $*p < 0.05$, $**p < 0.01$. C—pooled (calibrator) sample

cell cultures [47]. This could suggest a compensatory gene expression mechanism in the OFC and SFG, explaining the increase in gene expression identified in AD patients compared to non-demented controls.

As reviewed in Shankar et al. [48], progressive synaptic deterioration has been linked to AD pathology as well as cognitive deficits in several studies, which could explain the regional differences in expression in the three connected brain

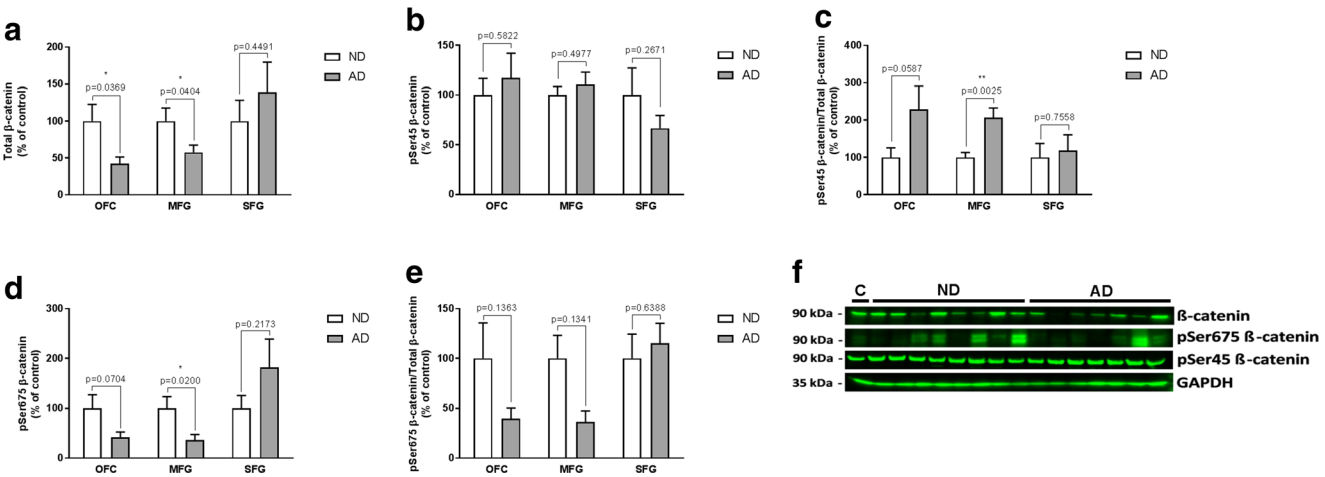

Fig. 8 Total level and phosphorylation of β-catenin. Western blot and quantification of **a** total β-catenin and its post-translational modifications on its **b** degradation directed phosphor-ser45 (pSer45 β-catenin) site and its **d** nuclear translocation site phosphor-Serine675 (pSer675 β-catenin). **c** and **d** shows the post-translational modification intensities normalized to total GSK3β protein. **f** Depict a minor representation of immunoblots of non-demented controls (ND) and Alzheimer's disease (AD) patients. Quantification of protein band intensities is normalized to GAPDH. Bar graphs shows % protein of ND (white) compared to AD (gray). Data depict mean ± SEM. $*p < 0.05$, $**p < 0.01$. C—pooled (calibrator) sample

Table 4 Correlation between gene and protein expressions

		OFC		MFG		SFG	
CTNNB1	Total β-catenin	0.418	0.066[a]	−0.170	0.486[a]	0.396	0.084[a]
	β-catenin S45/total	−0.408	*0.041*[a]	−0.088	0.721[a]	0.268	0.254[a]
	β-catenin S675/total	−0.111	0.652[a]	0.447	0.063	−0.221	0.394
GSK3B	Total GSK3β	−0.267	0.268	0.083	0.728	−0.119	0.627[a]
	GSK3β S9/total	0.212	0.383[a]	−0.065	0.787[a]	0.049	0.842[a]
	GSKβ Y216/total	0.035	0.885	0.041	0.865[a]	0.009	0.972[a]
RHOA	Total RHOA	0.338	0.158	−0.299	0.243[a]	0.140	0.556
WIF1	Total WIF1	0.252	0.298	0.055	0.826	−0.294	0.236[a]
APC	Total APC	0.170	0.499[a]	0.341	0.196[a]	0.461	0.065[a]
FZD2	Total FZD2	−0.076	0.766	0.328	0.198[a]	0.383	0.117[a]
FZD3	Total FZD3	0.183	0.467	−0.105	0.669	−0.173	0.507
FOSL1	Total FOSL1	0.255	0.307	0.127	0.616[a]	−0.020	0.935
LRP5	Total LRP5	0.020	0.952[a]	−0.190	0.437[a]	−0.428	0.068[a]
WNT2B	Total WNT2B	0.052	0.850	0.190	0.437[a]	0.025	0.921[a]
WNT7B	29-kDa WNT7B	0.071	0.818	−0.436[a]	0.082	−0.075	0.798
WNT7B	39-kDa WNT7B	0.484	0.042[a]	−0.461[a]	0.065	−0.316	0.216

[a] Spearman's rho correlation. Otherwise Pearson

regions. Here, we report evidence of several alterations in Wnt signaling pathway which precedes the apparent aging effect in the PFC in AD patients, denoting Wnt alterations in AD pathology. The regional expression patterns revealed in this study together with previous findings in other brain regions [28, 29, 31] support the idea that the interconnectedness in fact could be compromised in AD; however, further studies are needed.

Wnt signaling pathogenesis in AD animal models and cell cultures has also been a subject of previous studies. In both human AD brains and transgenic mice, DKK1 levels have been found to be increased, causing tau phosphorylation and mediated cognitive deficits [24, 49]. Further, Aβ treatment in cultured rat hippocampal neurons has also resulted in increased DKK1 levels [50–52]. Similar treatment of cultured neurons caused increased GSK3β activity [53, 54]. Inhibition of GSK3β or Wnt3a activation reduced both levels of Aβ burden and enzymatic BACE1 activity in murine Neuro2a cells [55]. Wnt3a activation also augmented autophagy through the AMPK axis simultaneously inactivating GSK3β [56]. In a double transgenic animal model, lithium inhibition of GSK3β correspondingly decreased Aβ aggregates and Aβ oligomers and reduced astrogliosis and spatial memory [57], all being AD pathogenic hallmarks. A very recent study further showed that inhibition of Wnt signaling contributed to accelerated AD pathology in transgenic mice and AD like changes in wild-type mice, partly by increased GSK3β levels and increase in GSK3β activity [58]. Combined, these studies suggest that impaired Wnt signaling is implicated in AD pathogenesis and to some extent are translatable to findings in

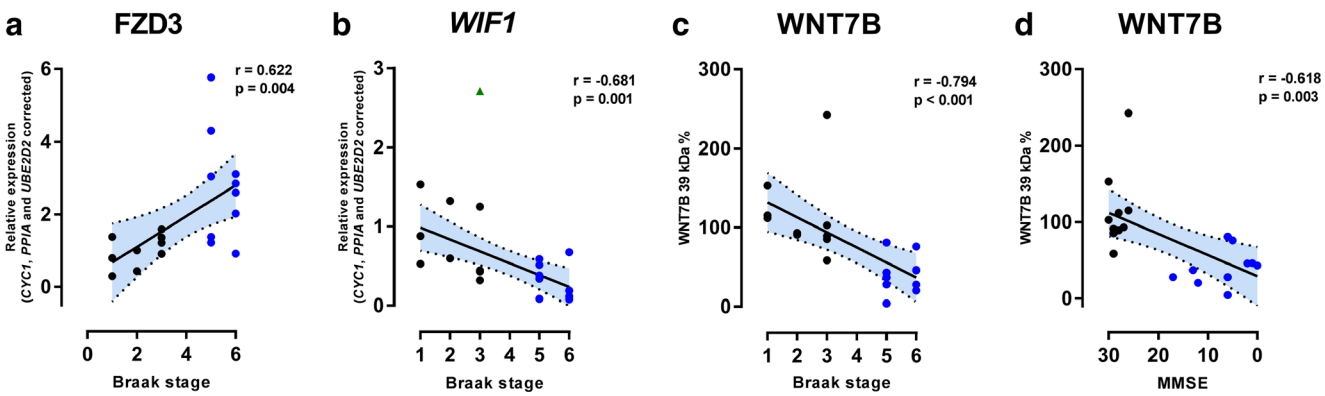

Fig. 9 Correlation between expression and Braak stage or Mini-Mental Examination State (MMSE). Significant correlation of gene expression of **a** *FZD3* and **b** *WIF1* and protein expression of **c** WNT7B in the orbitofrontal cortex during disease progression defined by post-mortem Braak staging and cognitive impairment assessed by the **d** MMSE. Black symbols: normal controls; blue symbols: Alzheimer's disease patients; green triangle: non-included outlier. r: Spearman's rho correlation. After Bonferroni correction, $p \leq 0.004$ is considered significant

humans. Similar differences in *GSK3B* and *LRP6* gene and protein expression levels were found in animal and cell culture as well as in human AD studies. Pei et al. found that active GSK3β correlated to the distribution of phosphorylated tau protein in AD brain [59]. Liu et al. [28] reported that *LRP6* mRNA and LRP6 protein levels were decreased in the temporal cortex of AD patients and were positively correlated to the levels of free β-catenin, which were also decreased in AD. Riise et al. [29] found decrease in total GSK3β and β-catenin levels in the hippocampus of AD patients. Those studies led us to evaluate the central proteins of Wnt signaling pathway, the GSK3β, and β-catenin. The GSK3β is a kinase involved in several pathways [60]. It is regulated by upstream kinases, PKA, and PKB/Akt [61], which by phosphorylation at tyrosine 216 (pTyr216) activates the kinase activity and phosphorylation at serine 9 (pSer9) inactivates the GSK3β kinase [34]. When activated, pTyr216-GSK3β phosphorylates β-catenin at Ser45 directing it for proteosomal degradation, otherwise β-catenin is phosphorylation at pSer675 which acts as a nuclear trafficking signal [62, 63]. We did not observe any differences in total GSK3β protein levels; however, the fraction of pTyr216-GSK3β of the total GSK3β was significantly increased in the OFC and MFG compared to controls, associated with a decrease in pSer9-GSK3β fraction in the OFC and a decrease of β-catenin levels. These results are in accordance with previous findings obtained by Leroy et al. [27]. Interestingly, no alterations of GSK3β and β-catenin were observed in the SFG; nonetheless, a significant increase in total GSK3α levels was shown. The neurological relevance of these observed changes remains to be elucidated. The activity of GSK3β has a clear effect on the levels and trafficking of its downstream target, β-catenin. We observed a significant decrease of total β-catenin levels in the MFG and OFC and a further increase in pSer45 fractions of β-catenin in the MFG and a borderline significance in OFC. The pSer675-β-catenin was visibly decreased, yet not statistically significant, in the MFG and OFC.

The results from this study are, to a certain extent, in agreement with a previous hypotheses and results, in which activated GSK3β is a reflection of inhibited Wnt signaling in AD patients [27]. However, it seems that regional differences in AD brains may be apparent; as the fraction of activated pTyr216-GSK3β in the hippocampus previously showed no differences, opposite to our results in the PFC [29] which is in accordance with previous work in the PFC by Leroy et al. [27]. On the other hand, previous work carried out by Caricasola et al. [24] found increased DKK1 protein in the temporal cortex and Riise et al. [29] found increased DKK1 gene expression in the hippocampus of AD cases. We however, did not observe any differences in all three areas. Liu-Chia Chen et al. [28] found LRP6 to be decreased in the temporal cortex, and Alarcon et al. [31] found a polymorphism variant of *LRP6* to be increased in AD patient. These results are not in compliance with our findings in the PFC, further supporting the idea of region specific pathology in AD.

The hypothesized Wnt signaling pathway inhibition reflected in the post-translational modifications of GSK3β and β-catenin is linked to several other pathological hallmarks in AD, namely, increased aggregation of neurofibrillary tangles [59, 64] and amyloid-beta plaques [65, 66], decreased cholinergic signaling [67, 68], and decreased hippocampal volume [69, 70]. Further studies have suggested that lithium, a GSK3β inhibitor, has a beneficial cognitive effect and a reducing effect on cerebrospinal pathological proteins in AD patients [71]. Combined, our study supports the idea that the Wnt signaling pathway including GSK3β may be a pivotal component and therapeutic target in AD pathology and progression.

In summary, we report that several gene and protein alterations are apparent in the prefrontal cortical structures of AD patients. A few genes related to the Wnt signaling pathway further appear to be correlated with the disease pathology and the cognitive performance. These changes are in accordance with the hypothesis of increased GSK3β activity in AD pathology, a molecular target in other neurological disorders.

Material and Methods

Braincloud™

Data used for the gene expression analyses during aging were obtained through the BrainCloud™ database (http://braincloud.jhmi.edu/) with courtesy of the Lieber Institute of Brain Development, Baltimore, MD, USA. Eighty-four genes were selected based on the subsequently used microarrays for Wnt pathway gene expression level analysis. We applied the analysis to 144 samples with a mean age of 45.4 years (range 21.0–78.2). The following genes, included in the Microarray analysis, were unavailable in the BrainCloud™: *JUN*, *MMP7*, *SFRP1*, *WNT2*, *WNT3*, and *WNT5A*. For *WNT2B* and *WNT4*, two transcripts named _1 and _2, respectively, were included in the analyses. The chromosomal location was assessed using the National Center for Biotechnology (NCBI) gene database.

Subjects

Snap-frozen, post-mortem, human brain samples from ten non-demented controls (age 81.0 ± 9.5, four male (M)/six female (F)) and ten AD diagnosed cases (age 81.9 ± 8.5, four M/six F) from MFG and ten non-demented controls (age 79.5 ± 8.9, six M/four F) and ten AD diagnosed cases (age 82.2 ± 5.4, three M/seven F) SFG were generously donated by the Netherlands Brain Bank (National Institute for Neuroscience, Amsterdam, Netherlands). Post-mortem brain samples of the OFC from ten non-

demented controls (age 85.4 ± 8.6, seven M/three F) and ten AD diagnosed cases (age 76.9 ± 9.3, four M/six F) were generously donated by the Banner Alzheimer's Institute (Banner Health Center, AZ, USA). Neuropathological reports including Braak staging for neurofibrillary tangles [3] were available for all samples. Sample groups were matched closely for sex, age, and post-mortem interval (PMI). Demographic data are summarized in Table S3. Clinical diagnosis of AD is based on the clinical criteria of probable AD [72, 73]. Only subjects older than 60 were selected for the study to minimize the inclusion of patients with familial AD. MMSE scores were only available for the OFC samples. Detailed neuropathological post-mortem evaluations were performed with informed consent from the donor or next of kind. All brain samples were collected and handled in accordance with Danish Ethical Standards of the Brain Banks and the Danish Health and Medicine Authorities. The study is approved by the Regional Ethical Committee, the Capital Region of Denmark, journal no. H-16031730. All samples were stored at − 80 °C prior to use. The samples from MFG were previously used to evaluate optimal reference genes and *GSK3B* as a validation target gene [74].

Tissue Handling and RNA Extraction

The RNA isolation and subsequent quantitative RT-qPCR was performed according to the minimum information for publication of quantitative real-time experiments (MIQE) guidelines [75]. All samples were handled using pre-chilled scalpels, collected in pre-chilled Eppendorf tubes, and used immediately in the RNA isolation protocol. Prior to RNA extraction, the brain samples were homogenized using MagNa Lyser (Roche Diagnostics, USA) and MagNA Lyser green beads (Roche, cat. 03358941001) at 2 × 6500 rpm for 25 s in 1-ml pre-cooled Qiazol. Total RNA extraction was performed using Qiagen RNeasy® Lipid Tissue Mini Kit (Qiagen, Cat. 74804) according to the manufacturer's instructions. In brief, the homogenized samples were mixed with 200-μl chloroform and the upper phase was transferred to a new tube and mixed 1:1 with 70% ethanol before loading onto purification columns. The RNA was eluted with 100-μl RNase/DNase-free water and then treated using the Turbo DNA-*free*™ kit (Ambion, cat. AM1907) or the First Strand kit genomic elimination kit (Qiagen, Cat. 330401) according to the manufacturer's instructions. RNA purity ($OD_{260/280}$ = 1.8–2.1) was determined using NanoDrop (Thermo Scientific, USA) [75]. RNA integrity was determined using Agilent 2100 bioanalyzer (Agilent Technologies, USA), and only samples with a RIN-value above 3.95 were subjected to further analyses [76]. RNA samples were stored at − 80 °C.

RT^2 Profiler cDNA Synthesis and PCR Arrays

cDNA was synthesized using the RT^2 First strand kit (Qiagen, Cat. 330401) using recommended 1 μg of total RNA pooled in sub-groups (matched for gender, age, and RIN) including five samples for each qPCR plate. Five extra samples of ND and AD from the SFG were implemented in RT-qPCR validation analysis. Prior to microarray analysis, the cDNA was additionally tested using a RT^2 profiler Quality Control PCR array (Qiagen, PAHS-999Z), designed to assess RNA quality. Relative mRNA expression of 84 genes was determined using the human Wnt signaling pathway RT^2 profiler PCR array (Qiagen, Cat. PAHS-043Z). Linearized relative expression levels were obtained using the $2^{-\Delta\Delta Ct}$ method [77] and the online software designed for the array (http://pcrdataanalysis.sabiosciences.com/pcr/arrayanalysis.php) and normalized to five reference genes. Gene expression levels with a negative and positive log2 FC ± 2 were considered for further validation by qPCR. The expression levels of following genes *FGF4*, *FOXN1*, *MMP7*, *PITX2*, *WNT16*, and *WNT3A* were under detection level and therefore excluded from further analyses.

Reverse Transcription and Quantitative PCR

Individual RNA samples were reverse transcribed using 200 ng of total RNA and the qScript cDNA SuperMix kit (Quanta, Cat. 95048), according to the manufacturer's instructions. A positive cDNA control used as a plate-to-plate calibrator was synthesized from the commercially available human universal reference total RNA (hRNA) (Clontech, Cat. 636538) using the same protocol. All samples were run in duplicates. RT-qPCR validations of microarray profiling hits were conducted for each individual sample using Fast SYBR® Green master mix (Applied Biosystems, Cat. 4385612) in 10-μl reactions on Stratagene MX3005p (Agilent Technologies, USA) qPCR instrument. The PCR thermal cycle conditions were initiated by 1 cycle of 20 s at 95 °C, followed by 40 cycles each consisting of 5-s denaturation step followed by varied annealing and/or acquisition step optimized for each primer pair (Table S4). Each run terminated with a melting curve analysis between 55 and 95 °C for qPCR product verification. The relative gene expression levels were normalized to the geometric mean of the following house-keeping genes *RPL13A*, *PPIA*, and *UBE2D2* (Table S1), as described previously [74]. The stability of the candidate reference genes was assessed with four different methods in combination: GeNorm [78], NormFinder [79], BestKeeper [80], and the comparative $\Delta\Delta C_t$ method [81] and evaluated in RefFinder (http://leonxie.esy.es/RefFinder/). Calculations of relative quantities were performed as

recommended by Hellemans et al. [82]. The expression levels of the following genes *FZD1*, *WISP1*, and *SOX17* were under detection level in more than 50% of individual samples and thus excluded from further analyses.

Tissue Homogenate Preparation

One hundred milligrams of brain tissue was added to 1-ml N-PER™ Neuronal Protein Extraction Reagent (Life Technologies, Cat. 87792) with pre-added 1:100 HALT™ Phosphatase Inhibitor Cocktail mix (Life Technologies, Cat. 788420) and 1:100 HALT™ Protease Inhibitor Cocktail mix (Life Technologies, Cat. 87786). The samples were then homogenized by pipetting followed by 10-s vortexing. The homogenates were incubated on ice for 10 min followed by centrifugation at 10,000 ×*g* for 10 min at 4 °C. The supernatant was collected, aliquoted, and stored at − 80 °C until further use. The protein concentrations were determined using Bradford Reagent (Sigma, cat. B6919) following the manufacturer's instructions. In brief, the protein samples were diluted 1:4 in N-PER™/HALT mix. The subsequent measurement of absorbance was performed on a Multiscan™ FC Microplate Photometer (Thermo Scientific, USA) at 620 nm using bovine serum albumin (BSA) (Sigma, Cat. A4503) as standard.

Immunoblotting

Equal concentrations of protein (20 μg) from each sample were dissolved in Pierce™ LDS Sample buffer, Non-reducing 4× (Life Technologies, Cat. 84788) containing DTT (100 mM) and heated up to 75 °C for 10 min. Samples were electrophoresed on pre-casted 17-well 4–20% SDS-PAGE gels (Expedeon, Cat. NXG42027K) and immediately transferred onto a PVDF Transfer Membrane (Thermo Scientific, Cat. 88518) using a semi-dry, BioRad apparatus (Bio-Rad Laboratories, Hercules, CA, USA) for 60 min, using a 200-mA/membrane constant current in 1× transfer buffer (Life Technologies, cat. NP0006-1). Membranes were blocked for 1 h in 5% dry-milk for non-phosphorylated proteins and 5% BSA for phosphorylated proteins before being incubated at 4 °C with primary antibodies overnight. Following washing step in PBS + 0.05% Tween-20, horseradish peroxidase (HRP) conjugated secondary antibodies were applied for 1 h at RT before adding HRP reactive SuperSignal® West Dura Extended Substrate (Thermo Scientific, Cat. 34075). The chemiflourecence was detected on Syngene Image Analyzer (Syngene, USA) and data was analyzed using Syngene Genetools software (Syngene, USA). Due to low levels, the proteins p-β-Catenin Ser45 and p-GSK3β Ser9 were detected using the secondary IRDye® flourophore-conjugated antibodies (Li-COR® biotechnology, UK) on LI-COR Odyssey FC infrared scanner. All samples were normalized to GAPDH as a reference protein, detected on a separate membrane, while pooled sample is used on each membrane as a calibrator for blot to blot variations (Fig. S2) as previously suggested by Taylor and Posch [83].

Antibodies

The following primary antibodies were used for immunoblotting: polyclonal anti-rabbit APC C-20 1:100 (Sc-896); polyconal anti-rabbit Fra-1/FOSL1 R-20 1:200 (Sc-605); polyclonal anti-goat FZD2 C-10 1:200 (Sc-68327); polyclonal anti-goat FZD3 H-20 1:200 (Sc-68333); polyclonal anti-rabbit LRP5 C-20 1:200 (Sc-21390); polyclonal anti-mouse Rho-A 26C4 1:200 (Sc-418); polyclonal anti-rabbit WIF-1 H-180 1:200 (Sc-25520); polyclonal anti-rabbit Wnt-2b H-39 1:100 (Sc-98737); polyclonal anti-goat Wnt-7b Q-13 1:100 (Sc-26363); monoclonal anti-mouse Gsk-3α/β 0011-A 1:200 (Sc-7291); polyclonal anti-rabbit p-Gsk-3β Tyr216 1:300 (Sc-135653); monoclonal anti-mouse β-catenin E5 1:200 (Sc-7963) (Santa Cruz Biotechnology, Inc., USA); p-β-catenin Ser675 D2F1 1:1000 (4176) (Cell Signaling Technologies, USA); and p-β-catenin Ser45 1:1000 (168-10277) (RayBiotech, Inc., USA). Protein samples were normalized to polyclonal anti-rabbit GAPDH FL-335 1:500 for HRP detection or 1:2000 (Sc-2577) (Santa Cruz Biotechnology, Inc., USA) for fluorescence detection. Secondary antibodies: HRP-conjugated secondary antibodies polyclonal goat anti-rabbit HRP (IgG H&L) 1:8000 (Ab97051); polyclonal goat anti-mouse HRP (IgG H&L) 1:8000 (Ab97023) (Abcam, USA); IR-Dye 800CW Goat anti-Rabbit IgG (# 926-32211; LI-COR Biosciences) 1:15,000; and IRDye® 680LT Goat anti-Mouse IgG1-Specific (# 926-68050; LI-COR Biosciences) 1:20,000.

Statistical Analyses

RT^2 Profiler PCR array data were analyzed in a non-statistical manner using the $2^{-\Delta\Delta Ct}$ method provided by the manufacturer. Data were tested for homoscedasticity using D'Agostino & Pearson Omnibus normality test and tested for equal variances using Levene's test. For statistical analyses, non-paired parametric Student's *t* test, one-way ANOVA, and Pearson correlation or Mann-Whitney rank sum test and Spearman rank correlation were performed using GraphPad Prism 6.0 (GraphPad Software, USA) or Real Statistics Resource Pack software v. 4.8. Heat maps are presented with individual correlation color scale based on Spearman's rho or log2 increments. The heat maps and hierarchical clustering are created using heatmap.2 function in gplots package in R version 3.3.1 (R foundation for Statistical Computing: http://www.r-project.org). Benjamini-Hochberg procedure was used for the BrainCloud™ analysis to account for false discovery

rate at 5%. Bonferroni was applied for multiple comparisons in post hoc analyses. Data are expressed by mean ± standard error of mean (SEM) or as box and whisker plots showing the minimum, the maximum, the median value, and the 25th, 50th, and 75th percentiles with a threshold of $p < 0.05$ considered to be statistically significant.

Data Availability The data underlying the findings using BrainCloud™ are fully available without restriction and available in the BrainCloud™ open-access platform and further available from the GEO Accession database (GSE30272).

Acknowledgements The authors are grateful to Hans-Jørgen Jensen and Rasmus Rydbirk for technical assistance.

Availability of Data and Materials The data analyzed during the current study is available from the corresponding author on reasonable request.

Authors' Contributions J.F. helped design the study, performed the experiments, analyzed and interpreted the data, and wrote the manuscript. T.B. designed the study, supervised the study and assisted with experimental design, data interpretation, and manuscript preparation. B.P supervised the project and assisted with manuscript preparations. All authors discussed the results and commented on the manuscript.

Funding Information This work was supported by the Dagmar Marshalls Foundation and Familien Hede Nielsens Foundation.

Compliance with Ethical Standards

Ethics Approval The Ethics Committee for the Copenhagen Regional Area approved this study (H-16031730).

Conflict of Interests The authors declare that there is no conflict of interest.

Abbreviations *AD*, Alzheimer's disease patients; *PFC*, prefrontal cortex; *CNS*, central nervous system; *M*, male; *F*, female; *NCBI*, National Center for Biotechnology; *OFC*, orbitofrontal cortex; *MFG*, medial frontal gyrus; *SFG*, superior frontal gyrus; *PMI*, post-mortem interval; *RT-qPCR*, reverse transcription quantitative real-time polymerase chain reaction; *MIQE*, the minimum information for publication of quantitative real-time experiments; *RIN*, RNA integrity number; *ND*, non-demented controls; *FC*, fold-change; *kDa*, kilodalton; p, phosphorylation; *Ser*, serine; *Tyr*, tyrosine; *MMSE*, Mini-Mental State Examination

References

1. Mayeux R, Stern Y (2012) Epidemiology of Alzheimer disease. Cold Spring Harb Perspect Med 2(8). https://doi.org/10.1101/cshperspect.a006239
2. Simic G, Kostovic I, Winblad B, Bogdanovic N (1997) Volume and number of neurons of the human hippocampal formation in normal aging and Alzheimer's disease. J Comp Neurol 379:482–494. https://doi.org/10.1002/(SICI)1096-9861(19970324)379:4<482::AID-CNE2>3.0.CO;2-Z
3. Braak H, Braak E (1991) Neuropathological stageing of Alzheimer-related changes. Acta Neuropathol 82:239–259. https://doi.org/10.1007/BF00308809
4. Masters CL, Multhaup G, Simms G, Pottgiesser J, Martins RN, Beyreuther K (1985) Neuronal origin of a cerebral amyloid: neurofibrillary tangles of Alzheimer's disease contain the same protein as the amyloid of plaque cores and blood vessels. EMBO J 4:2757–2763. https://doi.org/10.1002/j.1460-2075.1985.tb04000.x
5. Lindsay J, Laurin D, Verreault R, Hébert R, Helliwell B, Hill GB, McDowell I (2002) Risk factors for Alzheimer's disease: a prospective analysis from the Canadian Study of Health and Aging. Am J Epidemiol 156:445–453. https://doi.org/10.1093/aje/kwf074
6. Launer LJ, Andersen K, Dewey ME, Letenneur L, Ott A, Amaducci LA, Brayne C, Copeland JRM et al (1999) Rates and risk factors for dementia and Alzheimer's disease: results from EURODEM pooled analyses. EURODEM Incidence Research Group and Work Groups European Studies of Dementia. Neurology 52:78–84. https://doi.org/10.1212/WNL.52.1.78
7. Rubin EH, Morris JC, Storandt M, Berg L (1987) Behavioral changes in patients with mild senile dementia of the Alzheimer's type. Psychiatry Res 21:55–62. https://doi.org/10.1016/0165-1781(87)90062-x
8. Petry S (1989) Personality alterations in dementia of the Alzheimer type: a three-year follow-up study personality. J Geriatr Psyctiatry Neurol 2:203–207. https://doi.org/10.1177/089198878900200406
9. Siddiqui SV, Chatterjee U, Kumar D et al (2008) Neuropsychology of prefrontal cortex. Indian J Psychiatry 50:202–208. https://doi.org/10.4103/0019-5545.43634
10. Logan CY, Nusse R (2004) The Wnt signaling pathway in development and disease. Annu Rev Cell Dev Biol 20:781–810. https://doi.org/10.1146/annurev.cellbio.20.010403.113126
11. Cadigan KM, Nusse R (1997) Wnt signalling: a common theme in animal development. Genes Dev 11:3286–3305. https://doi.org/10.1101/gad.11.24.3286
12. Mikels AJ, Nusse R (2006) Wnts as ligands: processing, secretion and reception. Oncogene 25:7461–7468. https://doi.org/10.1038/sj.onc.1210053
13. Inestrosa NC, Varela-Nallar L (2014) Wnt signaling in the nervous system and in Alzheimer's disease. J Mol Cell Biol 6:64–74. https://doi.org/10.1093/jmcb/mjt051
14. Budnik V, Salinas PC (2011) Wnt signaling during synaptic development and plasticity. Curr Opin Neurobiol 21:151–159. https://doi.org/10.1016/j.conb.2010.12.002
15. Ille F, Sommer L (2005) Wnt signaling: multiple functions in neural development. Cell Mol Life Sci 62:1100–1108. https://doi.org/10.1007/s00018-00
16. Shimogori T, Van Sant J, Paik E, Grove EA (2004) Members of the Wnt, Fz, and Frp gene families expressed in postnatal mouse cerebral cortex. J Comp Neurol 473:496–510. https://doi.org/10.1002/cne.20135
17. De Ferrari GV, Moon RT (2006) The ups and downs of Wnt signaling in prevalent neurological disorders. Oncogene 25:7545–7553. https://doi.org/10.1038/sj.onc.1210064
18. Marchand A, Atassi F, Gaaya A, Leprince P, le Feuvre C, Soubrier F, Lompré AM, Nadaud S (2011) The Wnt/beta-catenin pathway is activated during advanced arterial aging in humans. Aging Cell 10:220–232. https://doi.org/10.1111/j.1474-9726.2010.00661.x
19. Farr JN, Roforth MM, Fujita K, Nicks KM, Cunningham JM, Atkinson EJ, Therneau TM, McCready LK et al (2015) Effects of age and estrogen on skeletal gene expression in humans as assessed by RNA sequencing. PLoS One 10:1–22. https://doi.org/10.1371/journal.pone.0138347

20. Jessberger S, Clark RE, Broadbent NJ, Clemenson GD, Consiglio A, Lie DC, Squire LR, Gage FH (2009) Dentate gyrus-specific knockdown of adult neurogenesis impairs spatial and object recognition memory in adult rats. Learn Mem 16:147–154. https://doi.org/10.1101/lm.1172609
21. Karasik D, Rivadeneira F, Johnson ML (2016) The genetics of bone mass and susceptibility to bone diseases. Nat Rev Rheumatol 12:323–334. https://doi.org/10.1038/nrrheum.2016.48
22. The Cancer Genome Atlas Network, Muzny DM, Bainbridge MN, et al (2012) Comprehensive molecular characterization of human colon and rectal cancer. Nature 487:330–337. https://doi.org/10.1038/nature11252.Comprehensive
23. Berwick DC, Harvey K (2014) The regulation and deregulation of Wnt signaling by PARK genes in health and disease. J Mol Cell Biol 6:3–12. https://doi.org/10.1093/jmcb/mjt037
24. Caricasole A, Copani A, Caraci F, Aronica E, Rozemuller AJ, Caruso A, Storto M, Gaviraghi G et al (2004) Induction of Dickkopf-1, a negative modulator of the Wnt pathway, is associated with neuronal degeneration in Alzheimer's brain. J Neurosci 24:6021–6027. https://doi.org/10.1523/JNEUROSCI.1381-04.2004
25. Hooper C, Killick R, Lovestone S (2008) The GSK3 hypothesis of Alzheimer's disease. J Neurochem 104:1433–1439. https://doi.org/10.1111/j.1471-4159.2007.05194.x
26. Zhang Z, Hartmann H, Minh Do V, Abramowski D, Sturchler-Pierrat C, Staufenbiel M, Sommer B, van de Wetering M et al (1998) Destabilization of beta-catenin by mutations in presenilin-1 potentiates neuronal apoptosis. Nature 395:698–702. https://doi.org/10.1038/27208
27. Leroy K, Yilmaz Z, Brion JP (2007) Increased level of active GSK-3beta in Alzheimer's disease and accumulation in argyrophilic grains and in neurones at different stages of neurofibrillary degeneration. Neuropathol Appl Neurobiol 33:43–55. https://doi.org/10.1111/j.1365-2990.2006.00795.x
28. Liu CC, Tsai CW, Deak F, Rogers J, Penuliar M, Sung YM, Maher JN, Fu Y et al (2014) Deficiency in LRP6-mediated Wnt signaling contributes to synaptic abnormalities and amyloid pathology in Alzheimer's disease. Neuron 84:63–77. https://doi.org/10.1016/j.neuron.2014.08.048
29. Riise J, Plath N, Pakkenberg B, Parachikova A (2015) Aberrant Wnt signaling pathway in medial temporal lobe structures of Alzheimer's disease. J Neural Transm 122(9):1303–1318. https://doi.org/10.1007/s00702-015-1375-7
30. Zenzmaier C, Marksteiner J, Kiefer A, Berger P, Humpel C (2009) Dkk-3 is elevated in CSF and plasma of Alzheimer's disease patients. J Neurochem 110:653–661. https://doi.org/10.1111/j.1471-4159.2009.06158.x
31. Alarcón MA, Medina MA, Hu Q et al (2013) A novel functional low-density lipoprotein receptor-related protein 6 gene alternative splice variant is associated with Alzheimer's disease. Neurobiol Aging 34:1709.e9–1709.e18. https://doi.org/10.1016/j.neurobiolaging.2012.11.004
32. De Ferrari GV, Papassotiropoulos A, Biechele T et al (2007) Common genetic variation within the low-density lipoprotein receptor-related protein 6 and late-onset Alzheimer's disease. Proc Natl Acad Sci U S A 104:9434–9439. https://doi.org/10.1073/pnas.0603523104
33. De Sarno P, Li X, Jope RS (2002) Regulation of Akt and glycogen synthase kinase-3β phosphorylation by sodium valproate and lithium. Neuropharmacology 43:1158–1164. https://doi.org/10.1016/S0028-3908(02)00215-0
34. Bhat RV, Shanley J, Correll MP, Fieles WE, Keith RA, Scott CW, Lee CM (2000) Regulation and localization of tyrosine216 phosphorylation of glycogen synthase kinase-3beta in cellular and animal models of neuronal degeneration. Proc Natl Acad Sci U S A 97:11074–11079. https://doi.org/10.1073/pnas.190297597
35. Ma T (2014) GSK3 in Alzheimer's disease: mind the isoforms. J Alzheimers Dis 39:707–710. https://doi.org/10.3233/JAD-131661
36. Chen M, Do H (2012) Wnt signaling in neurogenesis during aging and physical activity. Brain Sci 2:745–768. https://doi.org/10.3390/brainsci2040745
37. García-Velázquez L, Arias C (2017) The emerging role of Wnt signaling dysregulation in the understanding and modification of age-associated diseases. Ageing Res Rev 37:135–145. https://doi.org/10.1016/j.arr.2017.06.001
38. Vallée A, Lecarpentier Y (2016) Alzheimer disease: crosstalk between the canonical Wnt/beta-catenin pathway and PPARs alpha and gamma. Front Neurosci 10:1–12. https://doi.org/10.3389/fnins.2016.00459
39. Colantuoni C, Lipska BK, Ye T, Hyde TM, Tao R, Leek JT, Colantuoni EA, Elkahloun AG et al (2011) Temporal dynamics and genetic control of transcription in the human prefrontal cortex. Nature 478:519–523. https://doi.org/10.1038/nature10524
40. Brodmann K (1909) Vergleichende Lokalisationslehre der Grosshirnrinde—in ihren Prinzipien dargestellt auf Grund des Zellenbaues. Barth, Leipzig, Leipzig
41. Liang WS, Dunckley T, Beach TG, Grover A, Mastroeni D, Ramsey K, Caselli RJ, Kukull WA et al (2008) Altered neuronal gene expression in brain regions differentially affected by Alzheimer's disease: a reference data set. Physiol 33:240–256. https://doi.org/10.1152/physiolgenomics.00242.2007
42. Podtelezhnikov AA, Tanis KQ, Nebozhyn M, Ray WJ, Stone DJ, Loboda AP (2011) Molecular insights into the pathogenesis of Alzheimer's disease and its relationship to normal aging. PLoS One 6(12):e29610. https://doi.org/10.1371/journal.pone.0029610
43. Humphries CE, Kohli MA, Nathanson L, Whitehead P, Beecham G, Martin E, Mash DC, Pericak-Vance MA et al (2015) Integrated whole transcriptome and DNA methylation analysis identifies gene networks specific to late-onset Alzheimer's disease. J Alzheimers Dis 44:977–987. https://doi.org/10.3233/JAD-141989
44. Davis EK, Zou Y, Ghosh A (2008) Wnts acting through canonical and noncanonical signaling pathways exert opposite effects on hippocampal synapse formation. Neural Dev 3:32. https://doi.org/10.1186/1749-8104-3-32
45. Rex CS, Chen LY, Sharma A, Liu J, Babayan AH, Gall CM, Lynch G (2009) Different rho GTPase-dependent signaling pathways initiate sequential steps in the consolidation of long-term potentiation. J Cell Biol 186:85–97. https://doi.org/10.1083/jcb.200901084
46. Huesa G, Baltrons MA, Gómez-Ramos P, Morán A, García A, Hidalgo J, Francés S, Santpere G et al (2010) Altered distribution of RhoA in Alzheimer's disease and AβPP overexpressing mice. J Alzheimers Dis 19:37–56. https://doi.org/10.3233/JAD-2010-1203
47. Zhang L, Bahety P, Ee PLR (2015) Wnt co-receptor LRP5/6 overexpression confers protection against hydrogen peroxide-induced neurotoxicity and reduces tau phosphorylation in SH-SY5Y cells. Neurochem Int 87:13–21. https://doi.org/10.1016/j.neuint.2015.05.001
48. Shankar G, Walsh D (2009) Alzheimer's disease: synaptic dysfunction and Aβ. Mol Neurodegener 4:1–13. https://doi.org/10.1186/1750-1326-4-48
49. Killick R, Ribe EM, Al-Shawi R et al (2014) Clusterin regulates β-amyloid toxicity via Dickkopf-1-driven induction of the wnt-PCP-JNK pathway. Mol Psychiatry 19:88–98. https://doi.org/10.1038/mp.2012.163
50. Purro SA, Dickins EM, Salinas PC (2012) The secreted Wnt antagonist Dickkopf-1 is required for amyloid -mediated synaptic loss. J

Neurosci 32:3492–3498. https://doi.org/10.1523/JNEUROSCI.4562-11.2012
51. Zhang X, Yin WK, Shi XD, Li Y (2011) Curcumin activates Wnt/β-catenin signaling pathway through inhibiting the activity of GSK-3β in APPswe transfected SY5Y cells. Eur J Pharm Sci 42:540–546. https://doi.org/10.1016/j.ejps.2011.02.009
52. Rosi MC, Luccarini I, Grossi C, Fiorentini A, Spillantini MG, Prisco A, Scali C, Gianfriddo M et al (2010) Increased Dickkopf-1 expression in transgenic mouse models of neurodegenerative disease. J Neurochem 112:1539–1551. https://doi.org/10.1111/j.1471-4159.2009.06566.x
53. Takashima A, Noguchi K, Michel G, Mercken M, Hoshi M, Ishiguro K, Imahori K (1996) Exposure of rat hippocampal neurons to amyloid-beta peptide (25-35) induces the inactivation of phosphatidyl inositol-3 kinase and the activation of tau protein kinase I/glycogen synthase kinase-3beta. Neurosci Lett 203:33–36. https://doi.org/10.1016/0304-3940(95)12257-5
54. Takashima A, Honda T, Yasutake K, Michel G, Murayama O, Murayama M, Ishiguro K, Yamaguchi H (1998) Activation of tau protein kinase I/glycogen synthase kinase-3beta by amyloid-beta peptide (25-35) enhances phosphorylation of tau in hippocampal neurons. Neurosci Res 31:317–323. https://doi.org/10.1016/S0168-0102(98)00061-3
55. Parr C, Mirzaei N, Christian M, Sastre M (2015) Activation of the Wnt/β-catenin pathway represses the transcription of the β-amyloid precursor protein cleaving enzyme (BACE1) via binding of T-cell factor-4 to BACE1 promoter. FASEB J 29:623–635. https://doi.org/10.1096/fj.14-253211
56. Ríos JA, Godoy JA, Inestrosa NC (2018) Wnt3a ligand facilitates autophagy in hippocampal neurons by modulating a novel GSK-3β -AMPK axis. Cell Commun Signal 16:15. https://doi.org/10.1186/s12964-018-0227-0
57. Toledo EM, Inestrosa NC (2010) Activation of Wnt signaling by lithium and rosiglitazone reduced spatial memory impairment and neurodegeneration in brains of an APPswe/PSEN1ΔE9 mouse model of Alzheimer's disease. Mol Psychiatry 15:272–285. https://doi.org/10.1038/mp.2009.72
58. Tapia-Rojas C, Inestrosa NC (2018) Wnt signaling loss accelerates the appearance of neuropathological hallmarks of Alzheimer's disease in J20-APP transgenic and wild-type mice. J Neurochem 144:443–465. https://doi.org/10.1111/jnc.14278
59. Pei JJ, Braak E, Braak H, Grundke-Iqbal I, Iqbal K, Winblad B, Cowburn RF (1999) Distribution of active glycogen synthase kinase 3beta (GSK-3beta) in brains staged for Alzheimer disease neurofibrillary changes. J Neuropathol Exp Neurol 58:1010–1019. https://doi.org/10.1097/00005072-199909000-00011
60. Patel P, Woodgett JR (2017) Glycogen synthase kinase 3: a kinase for all pathways? Curr Top Dev Biol 123:277–302. https://doi.org/10.1016/bs.ctdb.2016.11.011
61. Fang X, Yu SX, Lu Y, Bast RC, Woodgett JR, Mills GB (2000) Phosphorylation and inactivation of glycogen synthase kinase 3 by protein kinase A. Proc Natl Acad Sci U S A 97:11960–11965. https://doi.org/10.1073/pnas.220413597
62. Hino S, Tanji C, Nakayama KI, Kikuchi A (2005) Phosphorylation of β-catenin by cyclic AMP-dependent protein kinase stabilizes β-catenin through inhibition of its ubiquitination. Mol Cell Biol 25:9063–9072. https://doi.org/10.1128/MCB.25.20.9063
63. Park MH, Kim DJ, You ST, Lee CS, Kim HK, Park SM, Shin EY, Kim EG (2012) Phosphorylation of β-catenin at serine 663 regulates its transcriptional activity. Biochem Biophys Res Commun 419:543–549. https://doi.org/10.1016/j.bbrc.2012.02.056
64. Yamaguchi H, Ishiguro K, Uchida T, Takashima A, Lemere CA, Imahori K (1996) Preferential labeling of Alzheimer neurofibrillary tangles with antisera for tau protein kinase (TPK) I/glycogen synthase kinase-3 beta and cyclin-dependent kinase 5, a component of TPK II. Acta Neuropathol 92:232–241. https://doi.org/10.1007/s004010050513
65. Ly PTT, Wu Y, Zou H, Wang R, Zhou W, Kinoshita A, Zhang M, Yang Y et al (2013) Inhibition of GSK3β-mediated BACE1 expression reduces Alzheimer-associated phenotypes. J Clin Invest 123:224–235. https://doi.org/10.1172/JCI64516.224
66. Cedazo-Mínguez A, Popescu BO, Blanco-Millán JM, Akterin S, Pei JJ, Winblad B, Cowburn RF (2003) Apolipoprotein E and beta-amyloid (1–42) regulation of glycogen synthase kinase-3beta. J Neurochem 87:1152–1164. https://doi.org/10.1046/j.1471-4159.2003.02088.x
67. Hoshi M, Takashima A, Noguchi K, Murayama M, Sato M, Kondo S, Saitoh Y, Ishiguro K et al (1996) Regulation of mitochondrial pyruvate dehydrogenase activity by tau protein kinase I/glycogen synthase kinase 3beta in brain. Proc Natl Acad Sci U S A 93:2719–2723. https://doi.org/10.1073/pnas.93.7.2719
68. De Sarno P, Bijur GN, Zmijewska AA et al (2006) In vivo regulation of GSK3 phosphorylation by cholinergic and NMDA receptors. Neurobiol Aging 27:413–422. https://doi.org/10.1016/j.neurobiolaging.2005.03.003
69. de Barreda EG, Pérez M, Ramos PG, de Cristobal J, Martín-Maestro P, Morán A, Dawson HN, Vitek MP et al (2010) Tau-knockout mice show reduced GSK3-induced hippocampal degeneration and learning deficits. Neurobiol Dis 37:622–629. https://doi.org/10.1016/j.nbd.2009.11.017
70. Blalock EM, Geddes JW, Chen KC, Porter NM, Markesbery WR, Landfield PW (2003) Incipient Alzheimer's disease: microarray correlation analyses reveal major transcriptional and tumor suppressor responses. Proc Natl Acad Sci U S A 101:2173–2178. https://doi.org/10.1073/pnas.0308512100
71. Forlenza OV, Diniz BS, Radanovic M, Santos FS, Talib LL, Gattaz WF (2011) Disease-modifying properties of long-term lithium treatment for amnestic mild cognitive impairment: randomised controlled trial. Br J Psychiatry 198:351–356. https://doi.org/10.1192/bjp.bp.110.080044
72. Mckhann G, Drachman D, Folstein M, Katzman R (1984) Clinical diagnosis of Alzheimer's disease. View Rev 34:939–944. https://doi.org/10.1212/WNL.34.7.939
73. Dubois B, Feldman HH, Jacova C, DeKosky ST, Barberger-Gateau P, Cummings J, Delacourte A, Galasko D et al (2007) Research criteria for the diagnosis of Alzheimer's disease: revising the NINCDS-ADRDA criteria. Lancet Neurol 6:734–746. https://doi.org/10.1016/S1474-4422(07)70178-3
74. Rydbirk R, Folke J, Winge K, Aznar S, Pakkenberg B, Brudek T (2016) Assessment of brain reference genes for RT-qPCR studies in neurodegenerative diseases. Sci Rep 6:37116. https://doi.org/10.1038/srep37116
75. Bustin SA, Benes V, Garson JA, Hellemans J, Huggett J, Kubista M, Mueller R, Nolan T et al (2009) The MIQE guidelines: minimum information for publication of quantitative real-time PCR experiments. Clin Chem 55:611–622. https://doi.org/10.1373/clinchem.2008.112797
76. Weis S, Llenos IC, Dulay JR, Elashoff M, Martínez-Murillo F, Miller CL (2007) Quality control for microarray analysis of human brain samples: the impact of postmortem factors, RNA characteristics, and histopathology. J Neurosci Methods 165:198–209. https://doi.org/10.1016/j.jneumeth.2007.06.001
77. Livak KJ, Schmittgen TD (2001) Analysis of relative gene expression data using real-time quantitative PCR and the 2(−delta delta C(T)) method. Methods 25:402–408. https://doi.org/10.1006/meth.2001.1262

78. Vandesompele J, De Preter K, Pattyn F et al (2002) Accurate normalization of real-time quantitative RT-PCR data by geometric averaging of multiple internal control genes. Genome Biol 3:1–11. https://doi.org/10.1186/gb-2002-3-7-research0034
79. Andersen CL, Jensen JL, Ørntoft TF (2004) Normalization of real-time quantitative reverse transcription-PCR data: a model-based variance estimation approach to identify genes suited for normalization, applied to bladder and colon cancer data sets normalization of real-time quantitative reverse. Cancer Res 64:5245–5250. https://doi.org/10.1158/0008-5472.CAN-04-0496
80. Pfaffl MW (2004) Relative quantification. Real-time PCR 3:63–82. https://doi.org/10.1186/1756-6614-3-5
81. Silver N, Best S, Jiang J, Thein SL (2006) Selection of housekeeping genes for gene expression studies in human reticulocytes using real-time PCR. BMC Mol Biol 7:33. https://doi.org/10.1186/1471-2199-7-33
82. Hellemans J, Mortier G, De Paepe A et al (2007) qBase relative quantification framework and software for management and automated analysis of real-time quantitative PCR data. Genome Biol 8: R19. https://doi.org/10.1186/gb-2007-8-2-r19
83. Taylor SC, Posch A (2014) The design of a quantitative western blot experiment. Biomed Res Int 2014:361590–361598. https://doi.org/10.1155/2014/361590